Directional Notches as Microstructures to Promote Nucleation and Heat Transfer in Pool Boiling

Callum McLaughlin
cpm3111@rit.edu

Directional Notches as Microstructures to Promote Nucleation and Heat Transfer in Pool Boiling

By

Callum McLaughlin

A Thesis Submitted in Partial Fulfillment of the Requirements for the

Degree of Master of Science in Mechanical Engineering

Committee Approval

Approved: _____ Date:_____

Dr. Satish G. Kandlikar

Department of Mechanical Engineering

(Thesis Chair)

Approved: _____ Date:_____

Dr. Michael Schrlau

Department of Mechanical Engineering

(Department Representative)

Approved: _____ Date:_____

Dr. Stephen Boedo

Department of Mechanical Engineering

(Examiner)

Approved: _____ Date:_____

Dr. Ke Du

Department of Mechanical Engineering

(Examiner)

RIT

Directional Notches as Microstructures to Promote Nucleation and Heat Transfer in Pool Boiling

By

Callum McLaughlin

A Thesis Submitted in Partial Fulfillment of the Requirements for the

Degree of Masters of Science in Mechanical Engineering

Department of Mechanical Engineering

Kate Gleason College of Engineering

Rochester Institute of Technology

Rochester, New York 14623

September 2019

Abstract

Heat generation in electronic hardware has become a major limiting factor in achieving maximum efficiency in modern computer parts. Classically forced flow convection systems are used to remove this heat at high rates but can be costly to implement and can take up space that may be needed for other critical components. In response to this, systems that use fewer parts scale in compact spaces are needed. In these situations, pool boiling as a heat transfer mechanism can excel. Pool boiling removes heat through the evaporation of fluid. On a flat surface pool boiling is chaotic and this random nature may hinder its ability to remove heat as effectively. The surface geometry of a pool boiling system can be altered to direct the flow of generated vapor bubbles to allow for increased heat flow and higher heat transfer performance. By creating paths for the vapor to follow we can induce currents in the flow of cool fluid to the heater surface, creating a faster cycle of vapor production therefore cooling the heated surface at a faster rate.

The purpose of this study is to investigate angled chip notches as an alternative to already existing high heat transfer surfaces in pool boiling. These alternative chips may prove cheaper or easier to produce the alternative which may incorporate fine, hard to produce features or post process coatings like sintering and the addition of hydrophobic materials. This study will examine the effect these specifically designed notches have on the interaction between the directed vapor and the liquid pathways they create. By creating notches in the surface of the chip, vapor bubble is given sites to nucleate and form vapor pathways. The angle walls on the one side of the notch will act as a wedge when water being driven toward the notch pushes the nucleating bubble up and out of the notch. Combined with pairing nucleating notches up with another oppositely facing one the vapor bubble is departing earlier then it would have had it not been assisted by these surface elements. With just these paired notches placed in row, an HTC improvement of 158% was recorded, compared to a plain copper surface. With the inclusion of microchannels this improvement was brought up to 161%.

Acknowledgements

First, I would like to thank Dr. Kandlikar for inviting me into his lab and to do research under him. Working with him gave me a much clearer path during my grad program than I had when coming in. This took a good deal of stress off and allowed me to focus on my education and thesis. Also being introduced to different people in the research world through Dr. Kandlikar gave me better insight into the workings and interconnectedness of the academic world.

Also, thank you to the other members of my thesis committee, Dr. Michal Schrlau, Dr. Stephen Boedo, and Dr. Ke Du, for taking your time to review and critique my thesis proposal and for allowing me to present my finished thesis.

My tests would also not have been possible without the manufacturing talent of Craig Arnold and Rick Wurzer who brought my design into the real world. Even with the minuscule scale of the components I needed for my work, Craig and Rick was able to deliver excellently made parts.

From the beginning my biggest help in the lab was Aranya Chauhan. He showed me the working of all of the lab equipment from when I first met him, before I even started doing research and was doing coursework with Dr. Kandlikar. Aranya was always available when I needed help with paperwork and forms like online orders through the college. I also received a lot of formatting help and access to helpful past research notes from Aranya.

Lastly, the other people in the lab who help me with odds and ends and for sitting in on my thesis presentation practice runs. I learned many small tips to make equipment function more smoothly from the lab group, as well as links to models and math to make my data management better. Also, to the people who came before me in the lab and designed a lot of the infrastructure to run the tests on.

Table of Contents

List of Figures

List of Tables

NOMENCLATURE

q =   Heat Flux (W/cm^2)

k   =   Thermal Conductivity (W/m-K)

T   =   Temperature (°C)

ABBREVIATION

CHF   =   Critical Heat Flux

CNC   =   Computer Numerical Control

HTC   =   Heat Transfer Coefficient

c.t.c.   =   Center to Center

1. INTRODUCTION

Modern computing is demanding more energy for large more elaborate calculations in an ever-shrinking space. As the computer becomes smaller and more powerful the energy demand and resulting heat creation grows in kind. Boiling allows for fast removal of heat as the phase change from liquid to gas consumes substantial energy. Boiling takes two main forms depending on the motion of the fluid. If the bulk fluid is being forced by an external mechanism like a pump or gravity across a heated surface it is called flow boiling. Flow boiling benefits from the constant introduction of cool fluid over the surface achieving very high heat flux. In certain situations, it may be too expensive or take up too much room to be able to incorporate the mechanical systems necessary to force the fluid over the heated element. In these cases, pool boiling becomes an effective means to cool the system. In pool boiling the water is stagnant and the only motion driving the fluid is from the creation of vapor and it rising out of the liquid. There are limitations to how much heat can be effectively extracted from a surface in pool boiling because the rate of bulk fluid reaching the surface is limited by several factors. The section following will describe the process and steps pool boiling takes as surface temperatures rise.

1.1. Pool Boiling

Pool boiling contains several distinct regions that follow a series of stages thought to be first considered by Nukiyama [1] and further refined by Farber and Scorah [2] and described as a physical interpretation seen in Figure 1. As heat rises the rate of vapor formation does as well and in turn alters the currents that are taken by fluid flowing in to replace the evaporated fluid. These initial experiments aimed to discern the relationship between wall temperature and heat flux and what physical properties caused it to vary so drastically as surface temperature claimed. Many of these older experiments used a fine wire as a heating element creating differences from the flat surfaces used normally today but did offer initial insight to the issues of vapor production chocking off the heated surface.
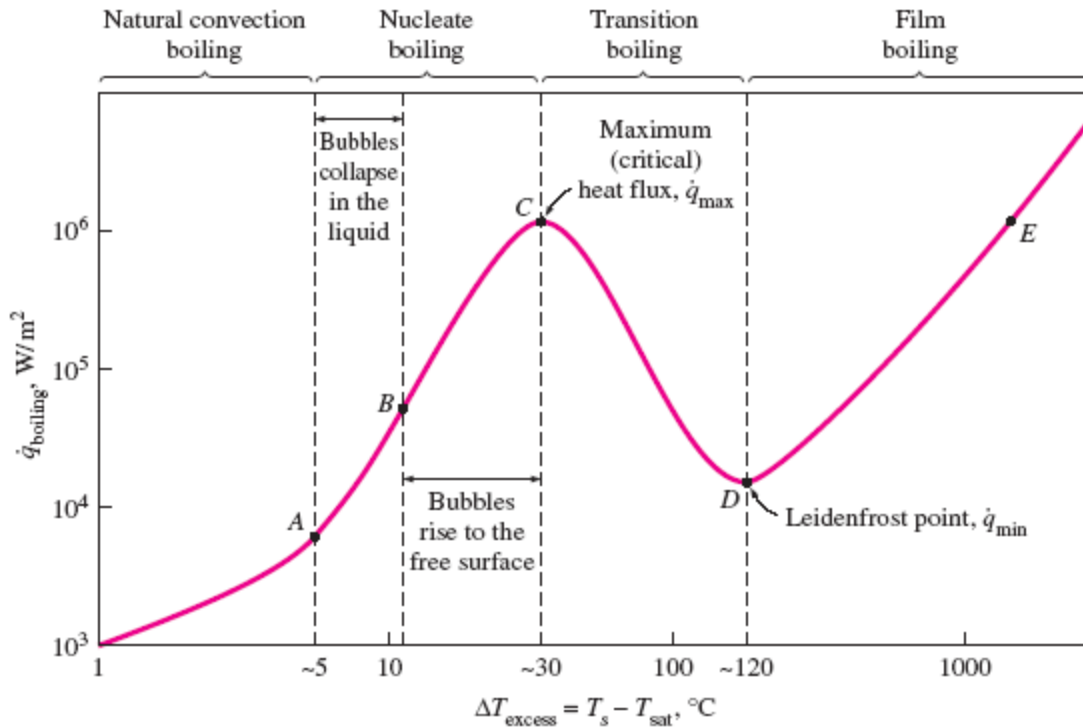
Figure 1 Physical Interpretation of Boiling Curve Faber and Scorch 1948

1.1.1. Natural Convection Boiling

As a fluid is heated, it first experiences heat transfer primarily through diffusion until it reaches a point defined by the Rayleigh number, after which it will experience movement due to a difference in density and enter the natural convection boiling region. This is a single phase heat transfer mechanism so no vapor will be formed. Heat flow is mainly from the exchange of less dense warm fluid rising up and denser cool fluid sinking down. These convection current's effectiveness far exceeds that of the heat diffusing through conduction.

1.1.2. Nucleate Boiling

In the second region past point A, bubbles will begin to nucleate on the heated surface. Point A is described as the Onset of Nucleate Boiling (ONB). After this point but before point B, vapor bubbles will form on the heated surface but not rise to the surface of the liquid, often collapsing if they leave the bottom since the liquid is too cold to maintain their vapor state. The temperature of the bulk fluid must be greater than the saturation temperature of the fluid for the pressure inside the vapor bubble for the bubble to grow or to

maintain its current size as it rises. Small crevasse in the material will act as nucleation sites. These crevices allow for gas to be trapped in the creating low pressure zones for bubble nucleation. At lower temperatures bubbles will require larger cavitation to be able to form. As the temperature continues to rise the areas that meet requirements for nucleation sites increases. With increased temperature bubbles no longer collapse while rising and make it to the surface. This begins the sub region seen after point B. This area sees the most dramatic change in turbulence of the fluid as bubble begin to rapidly depart the heated surface, quickly pulling water into the void they have created. Further heating sees bubbles forming columns and condensing into larger bubbles.

1.1.3. Transition boiling

Point C indicates the Critical Heat Flux (CHF) and the point where the vapor begins to interfere with the fluids ability to reach the heated surface. Without fluid contacting the surface as frequently, there is less heat being removed. As the surface temperature increases from lack of cooling, more areas on the surface begin to meet criteria for vapor production. This results in the surface becoming covered in larger patches of vapor reducing the transfer capability. Excessive heat will begin to build in the heated surface which may damage the components that where being cooled. In practical applications reaching CHF is not usually desired since it can hurt equipment, so cooling systems aim to stay below a safe range CHF while providing maximum heat transfer. Another goal of these pool boiling systems is to achieve the greatest heat flux at the lowest temperature, further protecting components from high heat. In the experiments performed in this study this region of the boiling curve will not be achieved. Instead once CHF has been hit, the boiling curve will move horizontally from the CHF peak to a point on the rising line in the film boiling region. This is because an electric heater is used to produce the heat in this experiment. The electric heater is controlled by a varying voltage input so no direct control over the surface temperature is possible. It is possible to achieve this region in a system that has direct control over the surface temperature such as by pumping temperature-controlled oil under the heated surface to maintain a constant temperature.

1.1.4. Film Boiling

After further increase in temperature the surface will entirely covered in vapor, the effectiveness of boiling in removing heat becomes negligible, and radiation takes over as the primary source of heat transfer. After this point D, the Leidenfrost point, film boiling insulates the fluid from the heated surface. The fluid will

now boil instantly upon contact with the surface and the vapor is hot enough to exceed the saturation temperature of the fluid therefore it is able to maintain a constant barrier of vapor. With the fluid unable to wet the heated surface HTC is greatly reduced and temperature will begin to spike. In the experiment performed, this region marks a runaway point as the voltage input will continuously increase the temperature with no way to quickly dissipate heat. Since the radiation will not be effective enough to remove excess energy the system will quickly approach dangerous temperatures which will mark the end of the experiments.

1.1.5. Separate Liquid Vapor Pathways

In order to increase the heat transfer coefficient and delay the onset of film boiling alterations to the heated surface can be made. One of the proven and basic examples is to increase surface area to allow for more regions through which your heat can pass into the fluid thereby increasing heat flux. Another method involves the deliberate placement of regions that encourage nucleation to direct vapor formation. With sperate nucleating and non-nucleating zones channels of vapor rising and fluid sinking can be formed. These separate regions, called liquid-vapor pathways, enhance flow rate of cool water to the surface increasing the heat transfer capable by the system and increasing CHF. As cool fluid contacts the surface in the non-nucleating zones it reduces the surface temperature in this region reducing the chance of nucleation as well as pre heating the fluid. Once a vapor bubble departs it creates a void that the fluid near the surface rushes into and evaporates. This bubble will depart and force new fluid downward continuing the cycle. The specific arrangement of these zones and the method by which the surface is enhanced to create them can drastically improve heat flux and CHF over a plain surface or surfaces with similar surface area but no organization.

Multiple methods exist for the purpose of creating separate liquid vapor pathways. These include, adding sintered metal regions to the top of the heated surface, altering the wettability of the surface through the application of hydrophobic and hydrophilic regions, and the addition of small surface fins in the form of microchannels. This study will use surface enhancements in the form of small engraved areas in the surface to produces nucleation sites in desired areas.

2. Literature Review

What is considered the first research into the phenomena of nucleate boiling was done between the World Wars by Mosciki and Broder [3] [4]. By heating a platinum wire in water, they found that the water temperature did not dictate the temperature at which the highest heat transfer was achieved. Later on, Nukiyama [1] would present the boiling curve that gave predictions for the process by which the state of nucleate boiling follows but was unable to connect the downward slope of the curve between the maxima and minima due to lack of ability to precisely alter wall superheat . The observation that there existed a thin layer in between the vapor bubble and surface was introduced by Hendricks and Sharp [5]. This micro fluid layer is fed from around the bubble and evaporates readily into the bubble increasing its volume and in turn increasing the contact region. They concluded that this mechanism accounted for most of the heat transfer seen in the system. Han [6] created a compressive explanation for heat transfer at a superheated surface. He found that when a vapor bubble departs the surface it pulls in liquid from around it in an area about twice the size of the departing bubble as well as how contact angle can determine bubble departure size. This new fluid would then undergo convection until a new vapor bubble was formed and repeated the process creating a forced fluid flow over the surface. With this, if the size and rate of bubble departure can be increased you can increase heat transfer from your surface, but the surface will still need to be able to be reachable by the incoming fluid.
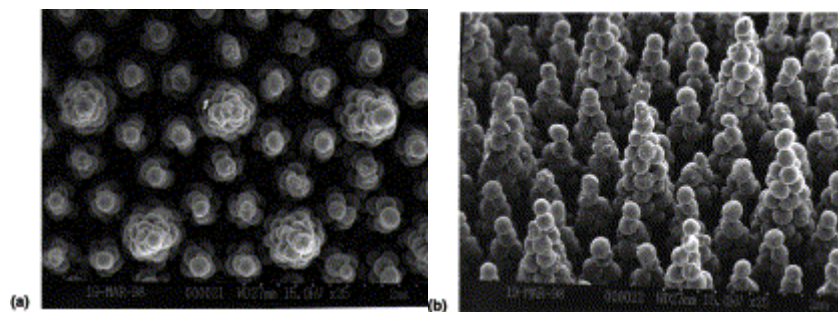
Figure 2 Micro stacks of sintered copper in a two height arrangement from [7]

Many studies have been done into the effects to nano and micro structures on heated surfaces to augment conditions for the improvement of heat transfer. While this study will be focusing on a scale of micro channels and the large-scale currents in the fluid they create, the nanostructure created by the surface finish are also of interest. Both of these surface enhancements help to combat the effects of film boiling. Novak Zuber [8] proposed that one of the mechanisms limiting nucleate boiling was that fluid flow was restricted from reaching the heated surface by the upward flow of vapor. He describes the stages the departing vapor

goes through before reaching a stage right before CHF where the bubbles have essentially coalesced into a single vapor jet. As a means of ensuring cool fluid reached the surface, Liter and Kaviany [7] created heated surfaces with strategically placed porous conical towers of sintered coper particles as seen in Figure 2 Micro stacks of sintered copper in a two height arrangement from . The towers would reach up into the bulk fluid supply and allow capillary action to draw cool fluid down toward their bases. Nucleation would then occur near the bottom of the pillars and vapor would rise around them. The efficiency of this setup was determined by the fluids ability to reach the base quickly and could be predicted by the viscous motion of the fluid though the sintered pillars. Although by building these relatively tall towers, 1mm to 1.8mm, add extra insulation to the top of the chips. Alternatively, Jaikumar and Kandlikar [9] cut channels into the surface of a copper chip. This created pathways for fluid to flow across the chip improving access at high temperatures when vapor flow begins to limit fluid access to certain areas. At set intervals equal to the critical capillary length for water at 100°C, intersecting microchannel where cut perpendicular to the rest. This provided further accessibility to cool fluid as vapor nucleates inside the microchannels. This study will follow closely to this Jaikumar and Kandlikar research using cut geometries in the surface to influence nucleation regions to drive a convective current down to the surface. But unlike the Jaikumar1 and Kandlikar study and another study by the same team [10], initially instead of using channels cut into a surface or fins, this study will guide the fluid current onto the machined chip surface itself. The fluid impacting the surface will then be driven at the divots pushing new cool fluid into the nucleation zones and preventing nucleation in the blank areas between the divot pairs. After the effectiveness of the notches in the surface was proven the addition of microchannels provided additional heat transfer and fluid flow similar to the effect seen in previous studies. Looking more directly at the dimensions of the channels, Dwight Cooke and Satish G. Kandlikar found the best performing channels tend to be "wide and deep" with the highest performing channel having a width of 375μm and depth of 400μm [11]. This 400μm is used in the majority of the chips produced in this study as both a width and depth. These dimensions showed the greatest results in this study as well. The remainder of chip dimensions and efficiency can be seen in table 1 and Figure 3 and Figure 4. The study also explains how the channel sizes alter vapor production and how incoming liquid supply id heated from three sides increasing its ability to cool the surface and preheat before nucleation faster than in other designs.

Table 1 Dimensions for chips used in [11]

Chip #	Channel width (μm)	Fin width (μm)	Channel depth (μm)	# of channels	Surface area augmentation factor
1	200	200	208	25	2.06
2	197	200	335	25	2.7
3	197	300	100	20	1.4
4	209	288	115	20	1.46
5	273	224	233	20	1.95
6	295	200	212	20	1.86
7	288	213	445	20	2.83
8	400	200	278	16	1.89
9	375	230	400	16	2.3
10	340	260	380	16	2.22
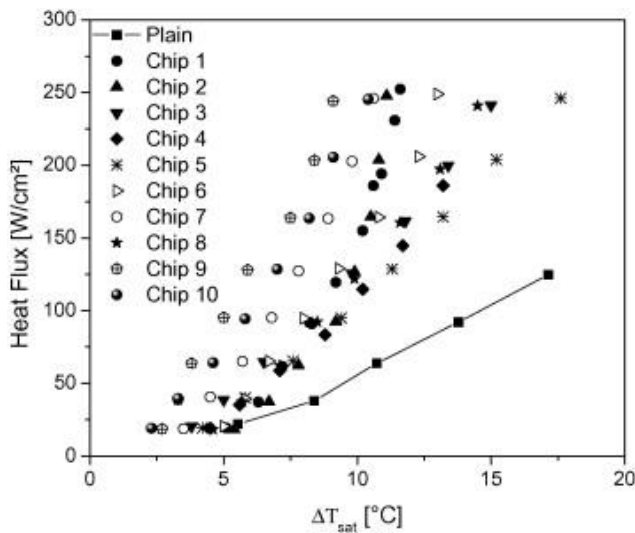
Figure 3 Heat Flux vs Wall super heat for chips in [11]
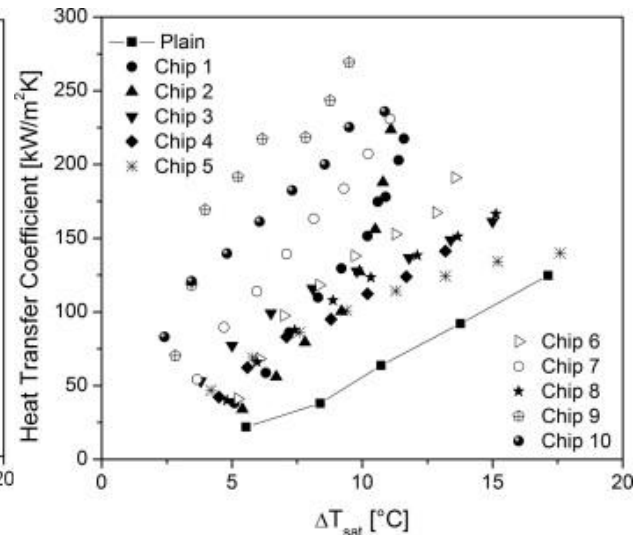
Figure 4 Heat Transfer Coefficient vs Wall Superheat for chips in [11]

Along with the blockage of fluid flow to the surface, the inability of a porous surface to reliably wet and fill voids left by departing vapor inhibits the effects of nucleate boiling and can result from vapor being trapped in the porous layer preventing the liquid from permeating the matrix. This can lead to worse performance from additional insulation and early film boiling [12]. To increase fluid flow through surfaces, several studies have worked with the nanostructure scale to arranges specifically designed nanostructures to increased wettability or combined porous surfaces with other mechanisms to allow for increased wetting. Shojaeian and Koşar [13] reviewed and concluded that while purposefully designed nanostructures alone

saw heat transfer improvement, many were lacking compared to what microstructures could achieve and was comparable to results from other less resource consuming methods such as sintered metal surfaces. Although some of the results from this review showed extremely positive enhancements both of which involved a series of crossing pathways and some form of tunnelways imbedded into the surface. The first of which used a copper mesh that had been laminated with several layers and cold rolled onto the surface of a copper chip [14]. This system had an increase of 27-fold in heat flux at low temperatures and pressure compared to a plain copper surface. They attribute the results to developing meshes with proper hole sizes allowing for fluid to easily flooding the heated surface. With finer mesh a steeper boiling curve is seen but with reduced CHF. The other study used a tube covered in a fish scale like surface with hollow pockets underneath to trap fluid [15]. Both of these studies along with the other nanoscale studies reviewed in [13] illustrated the importance of departing vapor not obstruction the rewetting mechanisms of the surface geometry. Imaging from this studies is show in Figure 5 Magnification of cold rolled mesh and cutaway [left], Scale like tube exterior and cutaway [right]. In contrasted much success is seen in very easily made, commercially available means. X.S. Wang, Z.B. Wang and Q.Z. Chen [16] describe the creation of porous surfaces through sintering and how these surfaces greatly enhance the heat transfer rate compared to a plain surface as long as the porous layer is not to thick. As an addition to the microstructure of fins with feeder channels, Patil and Kandlikar [17] added electrodeposited copper particles to just the tops of the fins. This encouraged nucleation on the tops of the fins over the low regions in the channels. Without nucleation in the channels the fluid flowed more freely through them, feeding the electrodeposited regions and further reducing nucleation in the channels. This was also the basis for the test in this study comparing the effect of sintered copper on the area between the pairs of notches while leaving the liquid pathway free of sintered copper. This aimed to recreate the effect of reducing nucleation in the free pathways and focus it into the area between the notches.
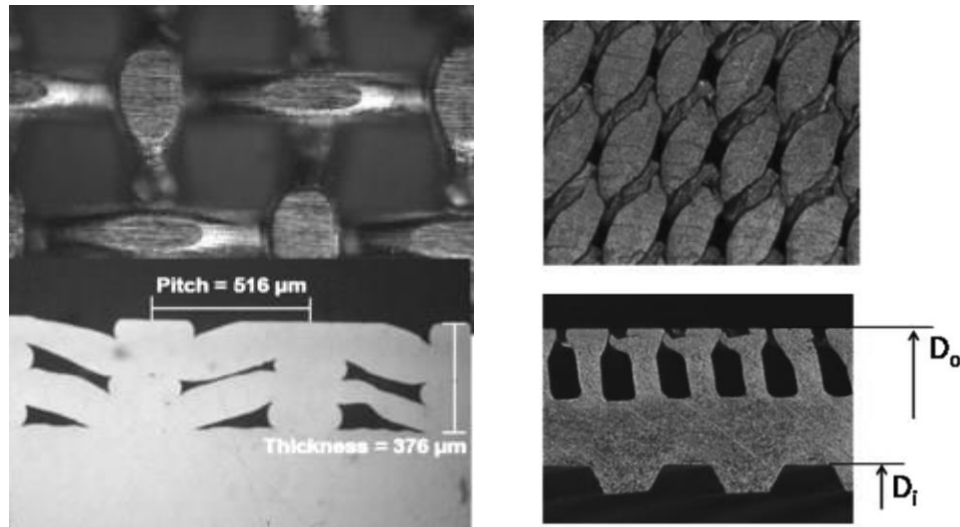
Figure 5 Magnification of cold rolled mesh and cutaway [left], Scale like tube exterior and cutaway [right]

Each notch is shaped in a way to impart force on the nucleation bubble such that it will move away from the vertical wall and up the ramp. At this scale the nucleation momentum [18] and the force of the incoming fluid as seen with similar shaped ramps on either side of fins by Kandlikar [19]. The production of these fins was very different involving a negative to be pressed into a blank and provided different constraints on dimensional control. In this study the ramp is positioned as close to the vertical wall as possible but is impeded by CNC machining capabilities.

Several other methods for augmenting the surface to improve CHF have yielded successful results in recent years. Austin Hayes' used additive manufacturing to create volcano like structures that acted like cooling towers by focusing steams of vapor up and out of the top and pulling cool water in from holes in the base [20]. These micro volcanoes printed on the top of the chip where able to increase CHF by 81%. Another is the augmentation of the contact angle through the usage of hydrophobic and hydrophilic areas. By creating a hydrophilic surface with a pattern of hydrophobic dots on top Betz et al. [21] saw an increase of CHF of 65% and a HTC increase of 100%. The hydrophilic surface increases surface wettability preventing vapor sheets from forming. The hydrophobic zones in turn promote nucleation by increasing the fluid contact angle and lowering the vapor pressure inside the nucleating bubble allowing for easier vapor formation. Recently the contact line of the fluid vapor interface has become a larger area of study such as [22] where shallow microchannel where used to increase the contact line region, to in turn increase CHF. On top of the normal evaporation, there is a significant amount of heat transfer through the microlayer of

fluid formed at the contact line around the base of the bubble. The vapor will not fully fill the microgrooves leaving fluid in the corners of the groove greatly increasing contact line area.
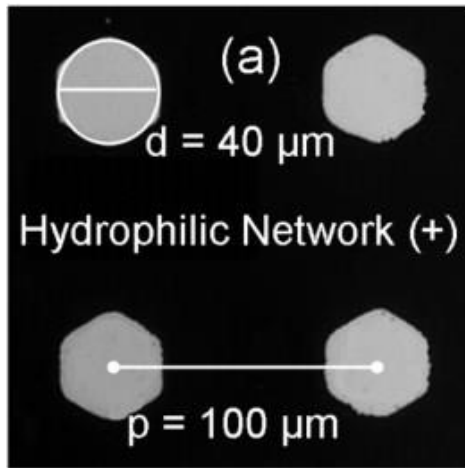

Figure 7 Spacing of hydrophobic [white] and hydrophilic [black] coating on surface from [21]
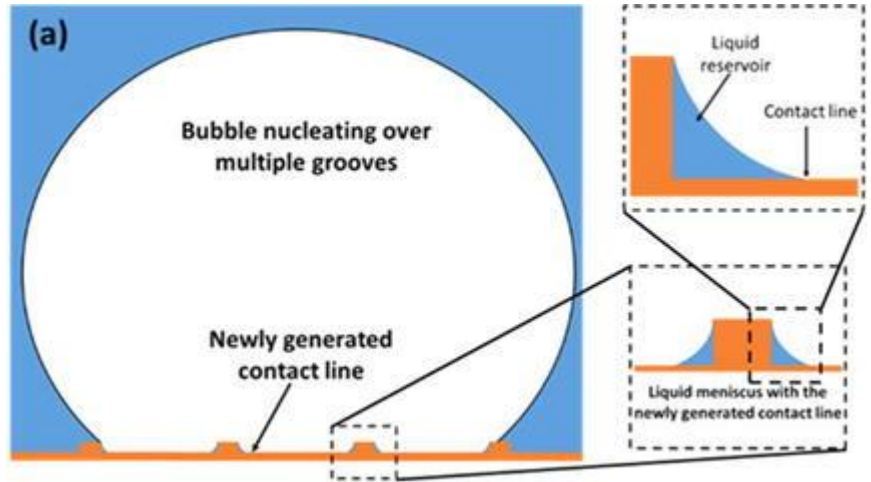
Figure 6 visual of how the vapor fluid contact line is altered by microchannels in [22]

3. Scope of Work

In this study novel geometry will be cut into the surface of pre-prepared copper chips in order to create separate liquid vapor pathways. Chips would then be tested for their heat transfer performance in a pool boiling setup. After initial designs were tested, new designs were created to reflect the success seen in the original chips. All of the chips where studied with a laser microscope to ensure correct dimensions and check surface roughness.

1. Manufacturing was performed using a CNC machine and microscale endmills. All designs are original with some dimensions based on successful trials in other pool boiling papers. Copper was chosen as the medium to construct chips from due to its high thermal conductivity and its availability and price. Copper has the downsides of oxidizing and having moderate machineability.

2. All chips are tested in the same pool boiling setup to study their HTC and CHF. During these experiments a Photrom FASTCAM 1024 PCI is used to capture high speed video of the nucleation. This allows for the measurement of bubble departure diameter which can be fed back into the chip design as well as visualizing the separate liquid vapor pathways.

3. All chips where measured using a Keyence VK-9700 violet laser scanning microscope to examine the surface roughness of the base chip as well as the machined surfaces cut into the chip. Roughness can be a major factor in nucleation so ensuring that the chips have similar surface roughness is necessary so that factor can be accounted when comparing results.

4. Experimental Work

4.1. Pool Boiling Setup

All chips were tested in a pool boiling apparatus shown in Figure 8. Figure 9 describes the components of the pool boiling apparatus. Each chip tested in this setup had the exterior dimensions depicted in Figure 17. The copper used had a conductivity of 391 W/m-K. Water was degassed using a pressure cooker method that is the same as the one described by [23]. Heat was generated by four 400W cartridge heaters running off of a voltage controller that where embedded in a large copper block with a column that came in contact with the bottom of the test chip. Sandwiched in between the chip and the heater was a thin sheet of graphite foil used to reduce the contact resistance between the two components. There is a fifth cartridge heater in the bulk fluid chamber to allow for heating up of the bulk as to hasten the onset of nucleation controlled by a separate voltage controller.

For temperature measurements three thermocouples were placed into the 3 holes drilled into the copper test chip. These thermocouples are labeled 1, 2, and 3 for the top, middle, bottom. The temperature reading for these thermocouples is represented by T_1, T_2, and T_3. A LabVIEW program recorded the temperature at these three points continuously. An increasing voltage was applied to the cartage heaters until nucleation was seen. From this point voltage would be increased in steps, the system was allowed to reach steady state, and then 10 seconds of temperature data was recorded. After this voltage would be stepped up again and this would repeat.

Heat flux was found using 1D heat transfer equation for Fourier's Law:

$$q'' = -k \frac{dT}{dx}$$

Temperature gradient was found using Taylor Series approximation as explained in [11]

$$\frac{dT}{dx} = \frac{3T_1 - 4T_2 + T_3}{2L_t}$$

L_t is the distance between the center of the thermocouples which in all tests was 3mm. After the heat flux is know we can calculate the wall super heat using the thermal conductivity of copper and the distance from the top thermocouple to the heated surface:

$$T_{wall\ superheat} = T_1 - \frac{q'' * L_s}{k} - 100°C$$

Here we are assuming the saturation temperature of the water to be 100°C. L_s is the distance from the center of the top thermocouple and the top surface. In all the chips this value is 1.7mm.
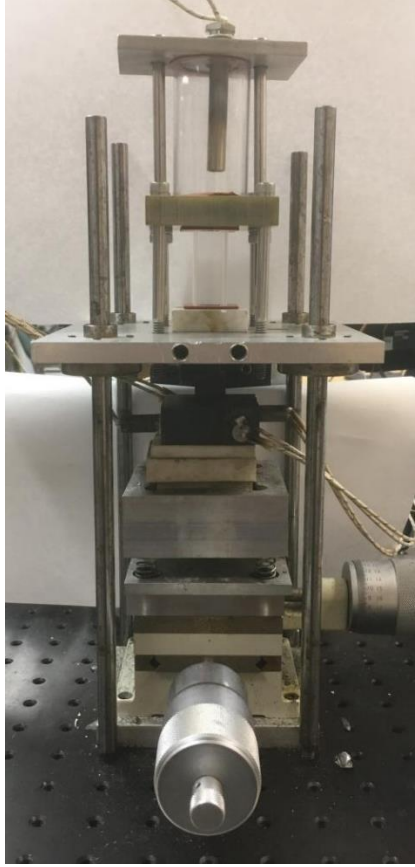
Figure 8. Pool Boiling Setup
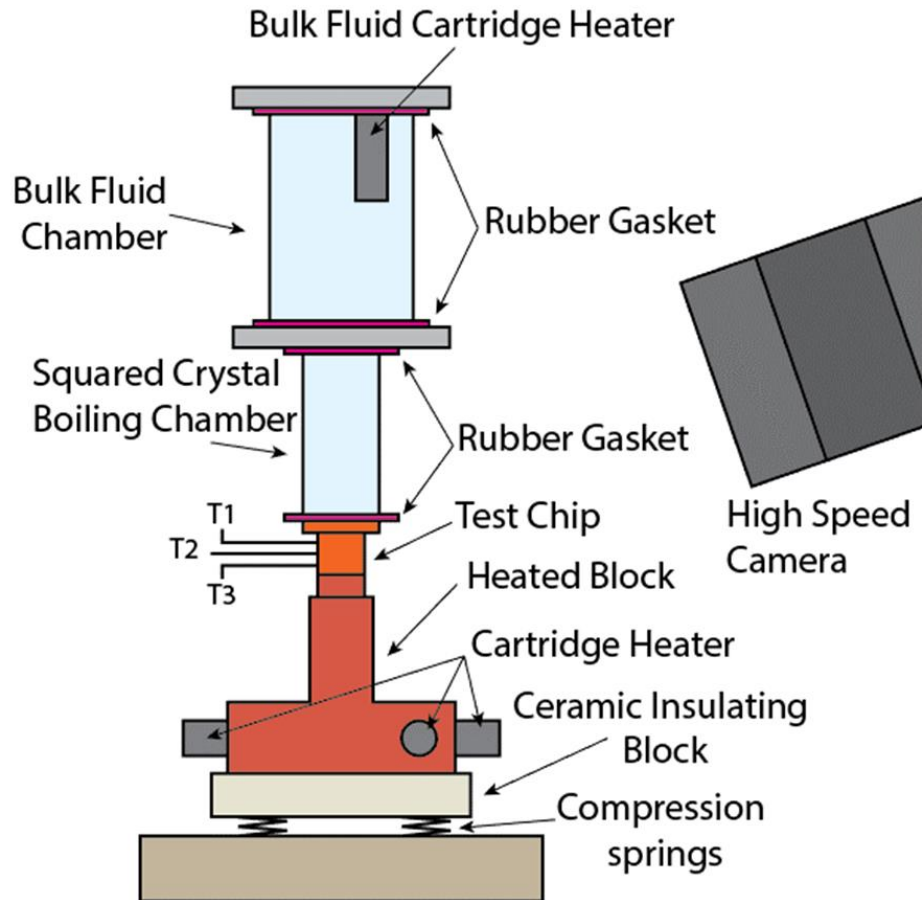
Figure 9 Diagram of Pool Boiling Experimental Setup

4.2. High Speed Camera

A Photrom FASTCAM 1024 PCI camera capable of speeds in excess of 10,000 fps was used for the high-speed photography. All highspeed was taken at 1000 fps unless otherwise noted. For the measurement of bubble diameter, a rod of known diameter was inserted into the test chamber and brought into focus. Using the diameter as a reference, bubbles in the same plane as the rod could be measured.

4.3. Design of Chips

Chips were first machined from copper blanks to match the dimensions is Figure 17 which is the standard base that is used for all of the tests. After machine work all chips where then cleaned with isopropyl alcohol to remove cutting fluid and any residual metal particles. After this several designs were created to be cut into the top surface to provide nucleation points. Optimally the chips where to be produced with a sharp 45-degree angle seen in Figure 10. Since this would be difficult to produce with the available techniques

it was instead decided to make geometries that would be possible with computer numerical control (CNC) machining. For this a rounded corner design with a flat floor was created as seen in Figure 11 Cutaway of first series of chip design. This general shape would be maintained across all the chip designs with variations on the notch spacing and width. This new 90-degree corner had relevant geometry to the study of vapor bubbles pushing from walls performed by Kandlikar [19]. Form this study we can see an unbalanced force is created forcing the bubble out way from the corner horizontally potentially driving it up the angled ramp in the divot. The purpose of the tightly grouped lines of paired divots in the sintered and un-sintered chips several purposes. Firstly, the small divots, instead of a line, could act as individual nucleation sites. They were also closely paired with the other groups such that any divot could contribute to neighboring vapor bubble with the ramp focusing them toward the center of the pair. With the pairs being in a row, the departing vapor, now in a curtain formation, would not interfere greatly with the incoming cool fluid. As the fluid flows down in between the vapor curtains it meets the chip surface and is forced into the side of the bubbles. This would provide a sweeping fluid flow over the surface increasing the amount of heat that could be carried away improving heat transfer though forced convection. The distance between the machined divots was chose based on [11] as the depth and width of the channels where decided based on the chip 8 design seen in Table 1 and guidance from Kandlikar. The design would hopefully encourage bubbles to form independently then merge once they passed a certain diameter. This new merged diameter would then depart quickly.
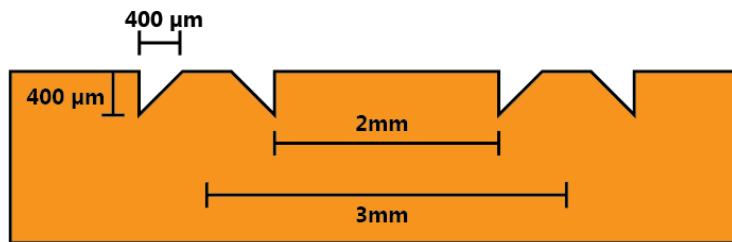
Figure 10 Originally theorized notch dimensions

The first set of chips was designed in a way to easily visualize the hypothesized merging bubbles. A single row of three sets of paired notches was cut into a chip creating the 3 Notch Pair chip. This provided a line of nucleation action that would develop into a 2D curtain of vapor. This way the high-speed camera with its narrow field of focus could hone in on just this section to be able to visualize the bubble merger. After the bubble merger was confirmed to be functioning as desired a second simple chip was made to see if these induced currents resulted in higher heat flux out of the chip resulting in the 9 notch pair chip.
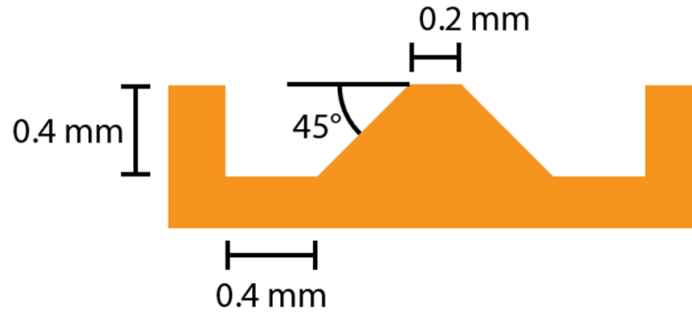
Figure 11 Cutaway of first series of chip design

The second set of chips was created to test the inclusion of a sintered strip in between the pairs of divots. Two chips where made with the same specifications so that one would act as a control while the other would have a thin line of sintered copper running in between the chips. For ease of applying the sintered row the space between the divot pairs was widened to 0.5mm. For the sintering application, after the chips were made, Kapton tape was used to cover over the holes and a mixture of two-parts 20 μm copper particle and one-part sintering oil was put into the areas not cover by tape. The tape was removed and the part was sintered at 450°C for 30 minutes and then again at 800°C for 1 hour. In addition to the spacing change a smaller end mill was purchased such that the back face of the divot could be made to include a flat section with the hope of increasing the force applied to the vapor bubbles pushing them toward the ramp. The sintered strip would provide nucleation site for lower wall superheat with the hope that a vapor curtain would form in this area first moving water and preventing nucleation in the areas between the pairs of notches.
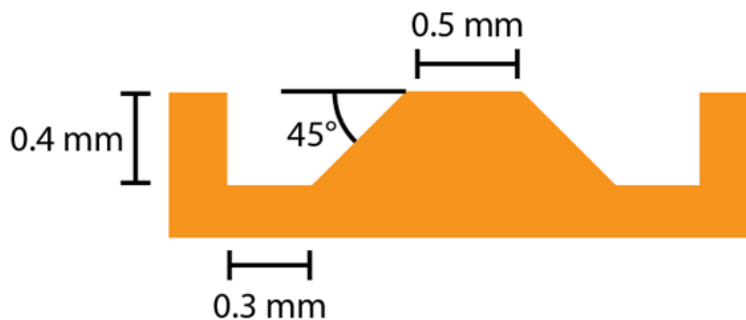
Figure 12 Sintered and un-sintered notch side profile

For the third iteration of chips it was decided to place the notches at the bottom of microchannel in order to create better flow regions. The short fins would help to guide fluid flow to the nucleating zones. The walls would also provide a surface for the vapor bubbles to adhere to. This would allow the vapor to vacate the notches allowing for new fluid to enter them. From issues with the un-sintered and sintered spacing, the ramps in the notches were brought together and the pairs of notches where spaced out to be 3mm apart.

Another chip was designed again with more space between pairs but instead of a 45° ramp a curved slope was used instead. The slope would allow for a tight nucleation zone like in the ramp notches while reducing the overall volume of the notch, forcing the vapor bubble to sit higher up on the surface. With more of the volume out of the notch the effect of the liquid stream driving the vapor columns together will have more surface area to act on pushing the vapor bubble together with more force.
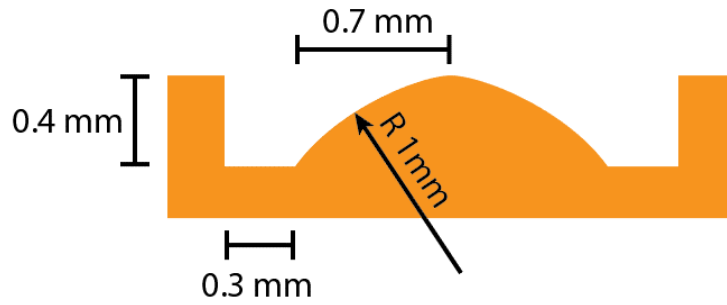
Figure 13 Curved slope notch side profile

The final design group involved the usage of microchannels with notches in the bottom of the channels to act as nucleation sites. The channels acted to direct water and allow continued access of water to nucleating regions from the bulk fluid to prevent the surface being chocked by vapor. The channels also act to cool the non-nucleating region to prevent unwanted boiling in this area as well as preheating the fluid before it reaches the nucleation zones. Three chips where produced with similar dimensions but different channel and wall widths. The chips had 300µm, 400µm, and 500µm wide walls and microchannels respectively. The better performing chip, the 400µm microchannel with notches chip, dimensions where used to make an integrated heater chip. This varied from previous designs as the heater block used to heat the base of the previous chip design would instead be integrated into the chip. This cuts down on thermal resistance and allows for greater heat flux though the surface of the chip without damaging the cartridge heater being used. Making this integrated heater chip was necessary as the previously used method for heating the microchannel chip was not able to achieve CHF in the microchannel chips.
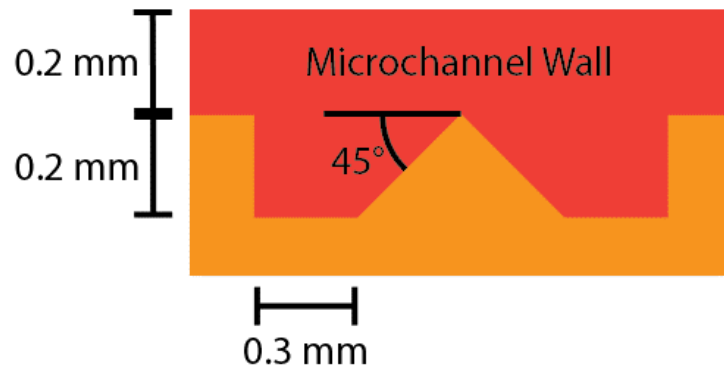
Figure 14 Microchannel with notches side profile

3 Notch Pair	9 Notch Pair	Un-sintered
Sintered	Curved Slope Notch	400µm Microchannels with Notches
300µm Microchannels with Notches	500µm Microchannels with Notches	Pitted Chip
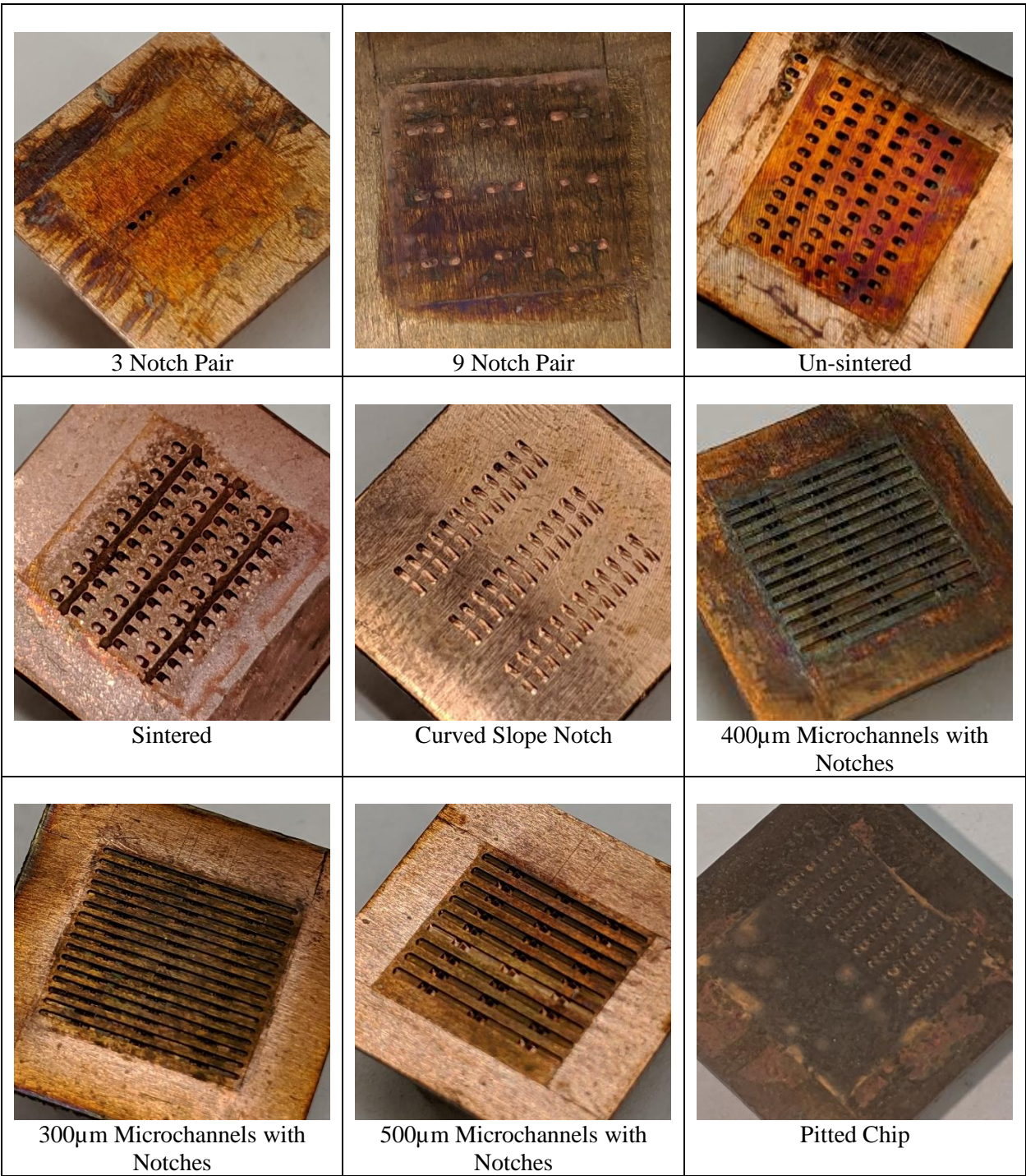
Figure 15 Images of all chips created for testing

Table 2 Notch Placement for all chips. Colum letter correspond to Figure 16 Guide for chip

Chip	Corner Radius (µm)	Slope Angle (°)	Distance between Paired Notches (mm)	Width of non-Nucleating Zones (mm)	Center to Center Distance of Paired Notches (mm)	Wall Thickness Between Notches (mm)	Number of Rows
			A	B	C	D	
3 Pair	200	45	0.2	0.7	2.5	N/A	1
9 Pair	200	45	0.2	0.7	2.5		3
Un-Sintered	150	45	0.5	0.5	2.5	0.4	12
Sintered	150	45	0.5	0.5	2.5	0.4	12
Curved Slope	150		0	1.6	3.6	0.4	12
300µm Micro	150	45	0	2	3	0.3	16
400µm Micro	150	45	0	2	3	0.4	12
500µm Micro	150	45	0	2	3	0.5	9
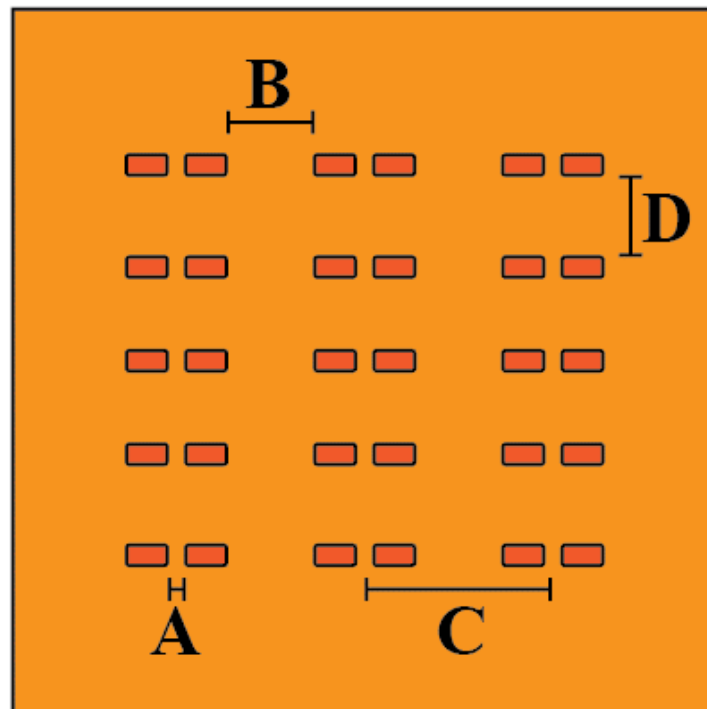
Figure 16 Guide for chip dimensions
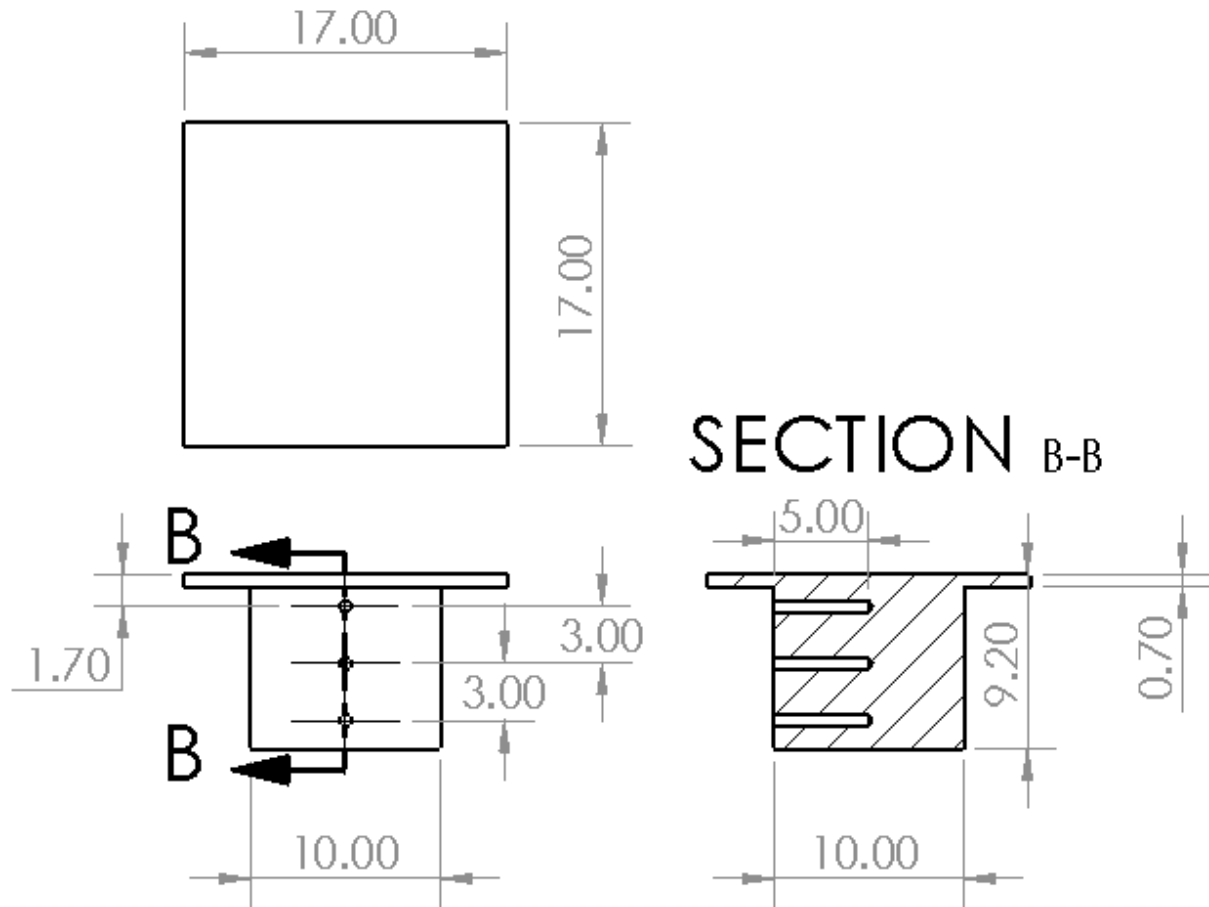
Figure 17 base chip dimensions (mm)

4.4. Laser microscope measurements

A laser scanning microscope was used to check the dimensions of the machined geometry. The microscope used was a Keyence VK-9700 violet laser scanning microscope capable of 4X, 10X, 50X and 150X magnification. For each chip a tilt correction was applied to ensure the scanned image was more level and a noise reduction was run on the normal setting to remove noise from the laser scan. Profiles for the pairs of notches was difficult to test as the magnification for fitting both into view was not accurate enough to see their geometry without major distortion so a 10X magnification was used for all chips. The software paired with the machine allowed for checking that the dimensions were correctly held as well as examining the roughness of the surfaces from the blank chip and milled areas.

Roughness calculations where done using arithmetical mean deviation.

$$Ra = \frac{1}{n}\sum_{i=1}^{n}|y_i|$$

In Table 3 Laser Scanning Microscope Measurments, Ra Surface describes the roughness of the flat surface of the chip while Ra Bottom describes the roughness of the surface at the bottom of the notch. Slope defines the angled portion of the notch with the target slope being 45°. The largest error in this slope was about 6% seen in the 9 notch pair chip. Notch width is the distance from side to side of the shorter distance of the notches. This measurement is perpendicular to the induced fluid/vapor flow. Notch depth describes the normal distance from the top surface of the chip, the heated surface, to the bottom of the notch while channel depth is from the top to bottom of the channel. The image in Figure 18 Scanning Laser Image of 400μm Microchannel with Notches Chip shows a resulting image from the laser scanning microscope with both color and contours drawn by the high measurements. The dark lines are not part of the actual color image and are drawn on by the software to emphasize high contours much like on a terrain high map.

Figure 18 Scanning Laser Image of 400μm Microchannel with Notches Chip 10x magnification
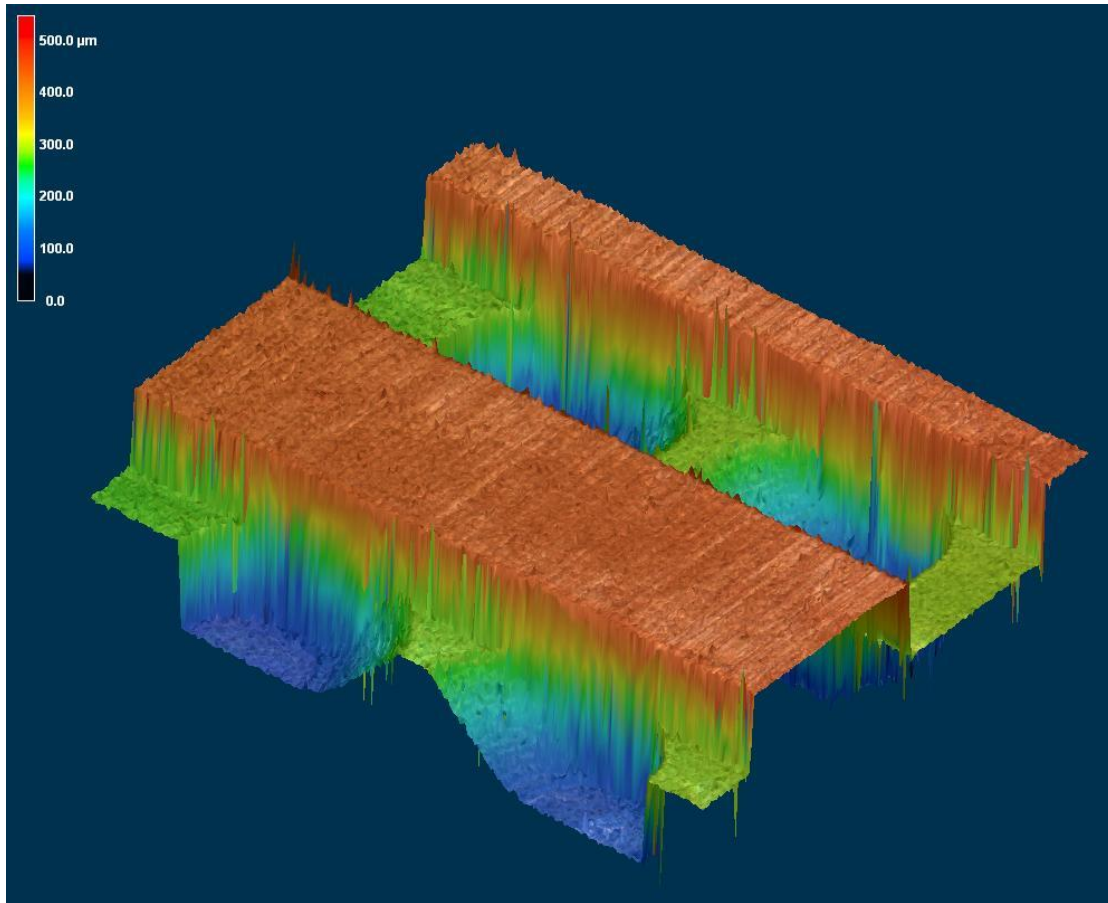
Figure 19 Scanning Laser Height Map of 400µm Microchannel with Notches Chip

Surface roughness plays a large part in the effectiveness of pool boiling. As shown in Walunj and Sathyabhama [24] as well as Jones et al. [25], the differences in roughness displayed in Table 3 Laser Scanning Microscope Measurments can have noticeable effect on the heat flux and max HTC. In both studies HTC rose as the roughness increased over the range from 1µm to 10µm on a flat surface undergoing pool boiling. In these measurements the 9 notch pair and sintered chips both had around double the roughness in their milled notches. This could contribute to a higher than normal HTC. In the 9 notch pair chip it isn't much concern as the chip was mainly used for a proof of concept. In the sintered chip the difference in effectiveness seen between it and its un-sintered counterpart is more so due to the addition of the sintered particles than the difference in roughness of the notches.

Larger discrepancies were present in the length and depth of the notches and channels. The width of notches was closer than any other element to their target value. Undercut measurements can be attributed to wear on the very small endmill which measured 300µm in diameter and the starting co-ordinates used on the CNC machine. Since the notches where sloped at one end, if the mill was set slightly too high this

would result in the depth of the notch being reduced but would also reduce the overall length. This can especially be seen in the magnified images of any chip that had touching slopes like in Figure 18 Scanning Laser Image of 400μm Microchannel with Notches Chip. In many of these the notches did not touch indicating that the end mill was too high. Since the width had no sloped walls it was affected far less by this issue which is important because the width and depth where the more crucial elements in the chip design.

The curved slope notch chip has no straight slope listed as it had a decreasing slope following the path of an arc of a circle. The nominal radius of the circle was set at 1mm. To check the actual value of the radius four points where taken. The points where taken in sets of three and used to solve for the determinants A, B, C, and D in the following which gives the equation for the circular slope.

$$A = \begin{vmatrix} x_1 & y_1 & 1 \\ x_2 & y_2 & 1 \\ x_3 & y_3 & 1 \end{vmatrix} \quad B = -\begin{vmatrix} x_1^2 + y_1^2 & y_1 & 1 \\ x_2^2 + y_2^2 & y_2 & 1 \\ x_3^2 + y_3^2 & y_3 & 1 \end{vmatrix} \quad C = \begin{vmatrix} x_1^2 + y_1^2 & x_1 & 1 \\ x_2^2 + y_2^2 & x_2 & 1 \\ x_3^2 + y_3^2 & x_3 & 1 \end{vmatrix} \quad D = -\begin{vmatrix} x_1^2 + y_1^2 & x_1 & y_1 \\ x_2^2 + y_2^2 & x_2 & y_2 \\ x_3^2 + y_3^2 & x_3 & y_3 \end{vmatrix}$$

Using these values, we can find the center position of the circle:

$$x_0 = \frac{-B}{2A} \quad y_0 = \frac{-C}{2A}$$

And then the radius can be found using:

$$r = \sqrt{(x_0 - x_1)^2 (y_0 - y_1)^2}$$

The four points taken results in six radii which the average of was 1.076mm. This falls into similar error range as the other machined dimensions.

Chip #	Chip Name	Ra Surface (µm)	Ra Bottom (µm)	Slope (deg)		Notch Width (µm)		Notch Length (µm)		Notch Depth (µm)		Notch Depth (µm)	
				Nom.	Act.	Nom.	Act.	Nom.	Act.	Nom.	Act.	Nom.	Act.
1	3 Pair	4.0	3.6	45.0	44.8	400.0	412.4	800.0	758.8	400.0	349.0		
2	9 pair	2.1	7.6	45.0	47.7	400.0	416.7	800.0	807.0	400.0	439.0		
3	un-sintered	2.1	3.1	45.0	45.4	400.0	399.5	700.0	719.5	400.0	392.0		
4	sintered	3.4	7.2	45.0	47.0	400.0	416.8	700.0	740.8	400.0	394.0		
5	curved slopes	2.5	3.9			400.0	390.6	1000.0	938.0	400.0	387.0		
6	microchannel 300µm	3.1	1.8	45.0	47.0	300.0	274.0	500.0	477.8	400.0	285.5	200.0	174.0
7	microchannel 400µm	5.0	2.4	45.0	43.8	400.0	373.9	500.0	502.0	400.0	355.0	200.0	162.0
8	microchannel 500µm	3.8	3.4	45.0	46.1	500.0	495.2	500.0	508.2	400.0	370.1	200.0	169.0
9	integrated	3.6	3.0	45.0	47.4	400.0	389.6	500.0	494.3	400.0	392.9	200.0	193.3

Table 3 Laser Scanning Microscope Measurments

5. Results

5.1. Uncertainty Analysis

Uncertainty present in the resulting data stems from the collection and processing of the heat flux data. An analysis was preformed to determine the bias and precision uncertainty present. For each experiment data was measured at each wall temperature point for 10 seconds at 10Hz to achieve a large enough sample size and mitigate random error. Uncertainty is comprised of two parts, bias and precision uncertainty. Bias uncertainty arises from the accuracy of the measuring instruments used in the experiment. The uncertainty of each instrument can often be found as a value given by manufactures that is checked for during production or though calibration done on the measurement devices. Bias uncertainty can be expressed generally as:

$$B_p = \sqrt{\sum_{i=1}^{n} \left(\frac{\partial p}{\partial \sigma_i} U_{\sigma_i} \right)^2}$$

Where B_p is the total bias uncertainty and U_{σ_i} is the uncertainty of each component of the final value. $\partial p / \partial \sigma_i$ represents the sensitivity coefficient that needs to be solved for each variable in the heat flux function. ∂p represents the change in the dependent variable, in this case q" and $\partial \sigma_i$ the independent variable that correlates with the uncertainty being expressed in this portion of the equation seen in Table 4 Sources of Uncertainty as Variable.

As shown in 4.1 the heat flux can be expressed as:

$$q'' = -k \frac{3T_1 - 4T_2 + T_3}{2L_t}$$

This function contains all of the variables whose uncertainties will combine to form the total uncertainty in the heat flux.

Table 4 Sources of Uncertainty

Item	Source of Uncertainty	Variable	Uncertainty
Thermal Conductivity of Copper	Varies over temperature range	k	9 W/m^{2}K [26]
Distance Between the thermocouples	Machining Error	L_t	127μm
Temperature at each thermocouple	Error in thermocouple reading	T_1, T_2, T_3	0.1K

The thermal conductivity of copper changes with temperature of the metal but in the chip there is a temperature gradient. For this reason, the largest a static number for thermal conductivity uncertainty that cover a range from room temperature to the highest operating temp is chosen. A worst possible case is chosen for all points so that the real value will fall inside this uncertainty range. Even with this the relative uncertainty of the thermal conductivity is <3%. We can expand out the general uncertainty formula with the uncertainty terms listed in the Table 4 Sources of Uncertainty.

$$\frac{B_{q''}}{q''} = \sqrt{\frac{\left(\frac{\partial q''}{\partial k} U_k\right)^2 + \left(\frac{\partial q''}{\partial L_t} U_{L_t}\right)^2 + \left(\frac{\partial q''}{\partial T_1} U_{T_1}\right)^2 + \left(\frac{\partial q''}{\partial T_2} U_{T_2}\right)^2 + \left(\frac{\partial q''}{\partial T_3} U_{T_3}\right)^2}{q''^2}}$$

Each of the sensitivity coefficients can be calculated using the function for heat flux.

$$\frac{\partial q''}{\partial k} = -\left(\frac{3T_1 - 4T_2 + T_3}{2L_t}\right) = \frac{q''}{k}$$

$$\frac{\partial q''}{\partial k} = -k\left(\frac{3T_1 - 4T_2 + T_3}{2L_t^2}\right) = \frac{-q''}{L_t}$$

Let $\alpha = 3T_1 - 4T_2 + T_3$

$$\frac{\partial q''}{\partial T_1} = -k\left(\frac{3}{2L_t}\right) = \frac{3q''}{\alpha}$$

$$\frac{\partial q''}{\partial T_2} = -k\left(\frac{4}{2L_t}\right) = \frac{-4q''}{\alpha}$$

$$\frac{\partial q''}{\partial T_3} = -k\left(\frac{1}{2L_t}\right) = \frac{q''}{\alpha}$$

So, the final expression for bias uncertainty can be written as:

$$\frac{B_{q''}}{q''} = \sqrt{\frac{\left(\frac{q''}{k} U_k\right)^2 + \left(\frac{-q''}{L_t} U_{L_t}\right)^2 + \left(\frac{3q''}{\alpha} U_{T_1}\right)^2 + \left(\frac{-4q''}{\alpha} U_{T_2}\right)^2 + \left(\frac{q''}{\alpha} U_{T_3}\right)^2}{q''^2}}$$

The precision uncertainty is expressed as standard deviation for discrete random variables in the form of:

$$P_{q''} = \sqrt{\frac{1}{N}\sum_{i=1}^{N}(x_i - \mu)^2}$$

Where

$$\mu = \frac{1}{N} \sum_{i=1}^{N} x_i$$

The Total uncertainty resulting from both the bias uncertainty and precision uncertainty is:

$$U_{q"} = \sqrt{P_{q"}^2 + B_{q"}^2}$$

Figure 20 Un-sintered Chip Total Uncertainty displays the total relative uncertainty for the un-sintered chip. This example reflects the trend of uncertainty through all other tests. Total uncertainty will rise but the relative uncertainty will exponentially decay until it drops below 5% where it begins to bottom out.
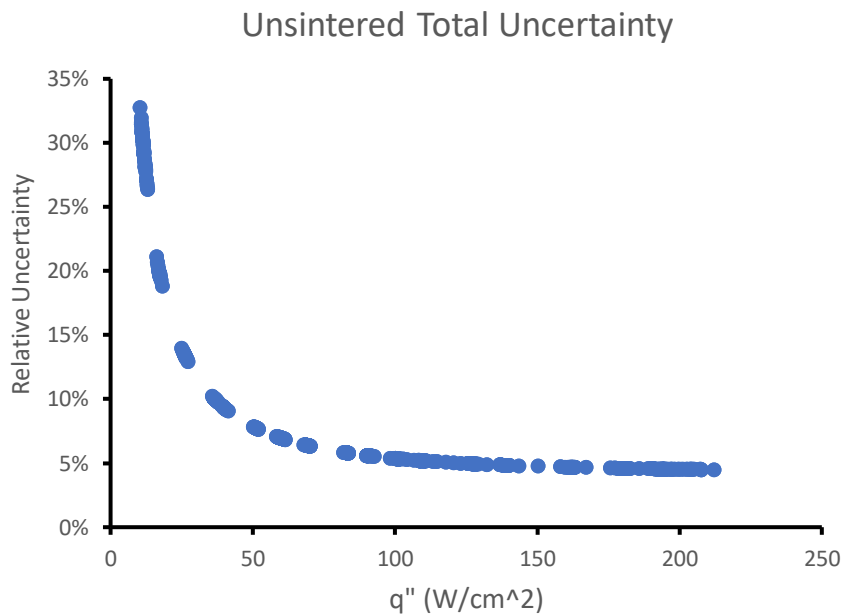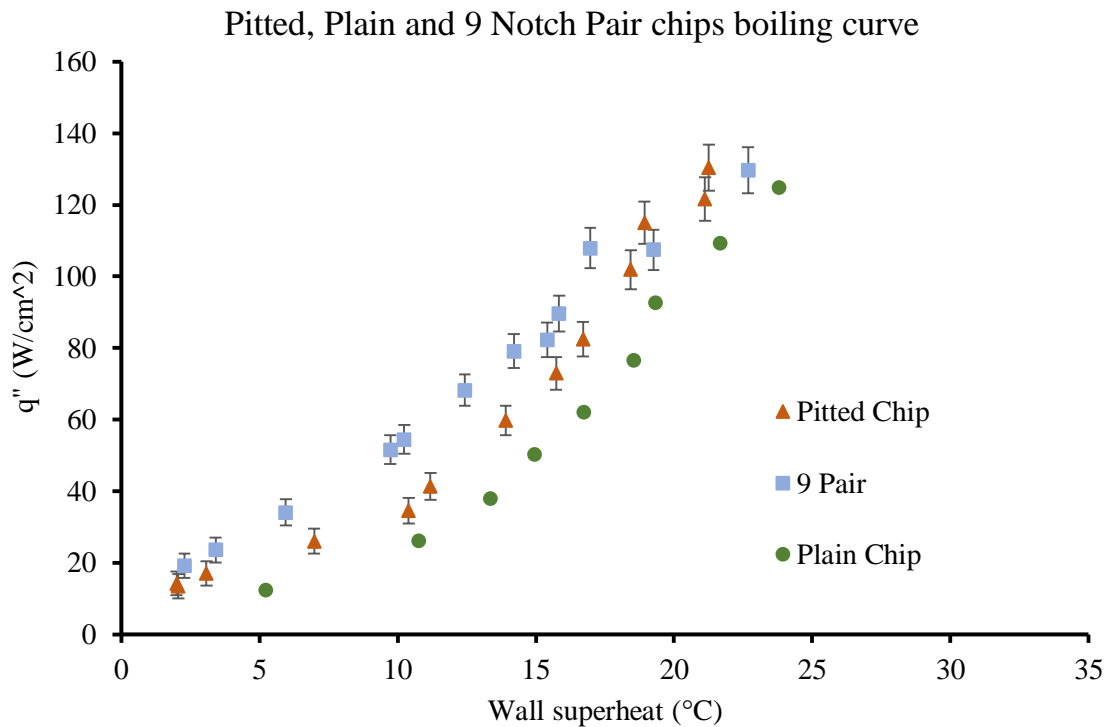

Figure 20 Un-sintered Chip Total Uncertainty

5.2. Chip Performance

The 3 Notch Pair chip in Figure 15 Images of all chips created for testing was the first chip created and tested. Results from the first test showed some improvement over a plain copper surface even with the simple geometry addition. The 3 Notch Pair chip also provided a single plane of bubble nucleation that allowed for easier photography of the merging bubbles. With these successful results, an additional 2 rows of paired notches where added resulting in the 9 Notch Pair chip Figure 21 shows the boiling curve for this chip, the plain chip and a chip from previous work used as a comparison. The chip used for comparison, the last chip shown in Figure 15 Images of all chips created for testing, had pits running across half of its

surface but the exact dimensions are unknown. The 3 Notch Pair chip was created for use in photography and no heat transfer data was taken. With only 3 pairs in a single plane it was easier to capture the bubble formation and departure and this was the chip used to produce the high-speed photography in Figure 31. It can be seen in Figure 21 that the chips with divots in their surface created a change in the boiling curve and increased the CHF slightly over the plain chip. Of note the 9 Notch Pair chip had a higher heat transfer than the pitted chip, despite the large difference in nucleation sites. Even with only 18 nucleation sites on the 9 notch pair chip as opposed to the 110 number of pits on the pitted chip the heat transfer was the same and sometimes better. This is significant as the cost of time to produce the 9 notch pair chip if both were machined would be much lower. The 9 Notch Pair chip can be seen hitting CHF slightly under 140 W/cm^2.

Figure 21 Pitted, Plain and 9 Notch Pair chips boiling curve

Figure 22 sintered and un-sintered boiling curve with uncertainty shows the results of the sintered and un-sintered chips. For each chip 2 experiments were run and the show graph is the composite of both those runs for each chip. Noticeably the sintered chip achieved CHF at a lower temperature and around 185 W/cm^2 while the unstirred hit CHF at around 200 W/cm^2. During the high-speed recordings for these tests it could be seen that the sintered strip running between the divot pairs was not performing as expected. Vapor bubbles did not sit on the sintered strip and it acted as a barrier between the two paired rows of divots causing bubbles to merge randomly with other rows ad well as their paired divots. This caused there to be

no distinct vapor pathways which may have lowered the effectiveness of the sintered chip. The un-sintered chip was not without its problems as vapor bubbles on during high speed recording were also seen merging with unpaired rows but to a lesser extent than in the sintered chip.
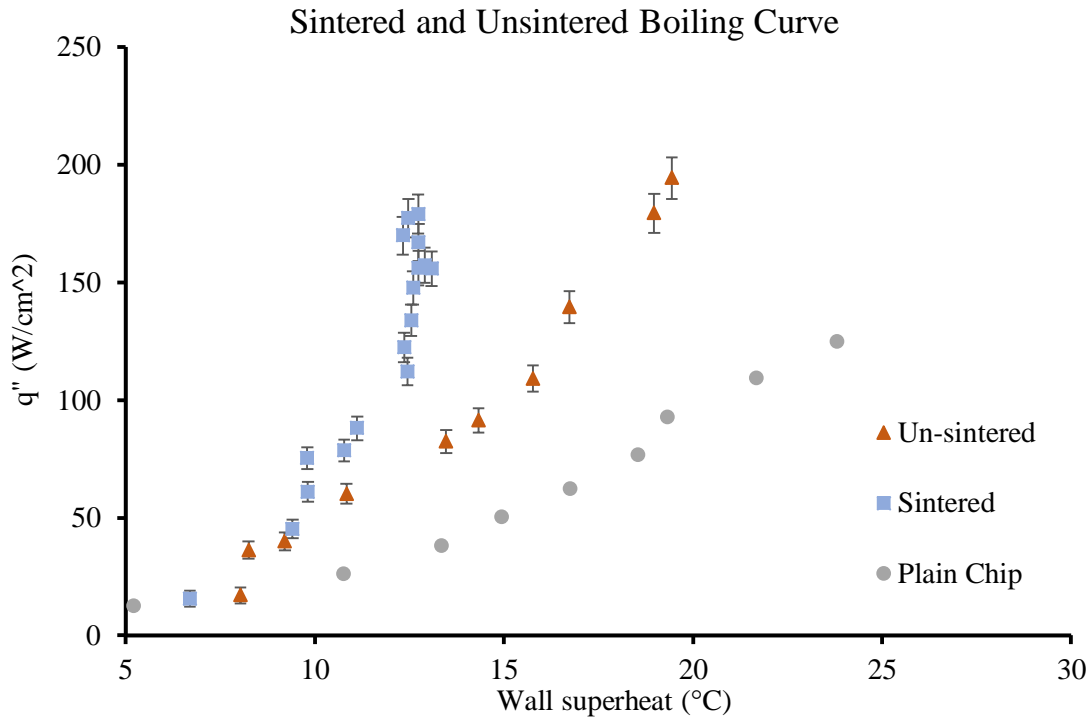

Figure 22 sintered and un-sintered boiling curve with uncertainty

In the next series of chips only one was fabricated and tested. Three experiment runs where performed with this chip. In all three runs the chip achieved CHF. Figure 23 Curved Slopes Notch boiling curve with uncertainty contains the combined data from the experiments performed with this chip. This curved slope notch chip achieved the greatest CHF of any chip up to this point, giving support to the effect of greater spacing between the pairs of notches. Compared to the issues with the sintered and un-sintered chip whose c.t.c. distance was 2.5 mm with a non-nucleating zone of width 0.5mm, this chip with its c.t.c. of 3.6 and non-nucleating region of 1.6 had more favorable results. Individual vapor curtains where more prevalent in this chip compared to others further supporting this increase in distance allowing bubbles to fully form and depart in their individual rows without margining with neighboring rows and disturbing the downward fluid flow. Despite the chip having longer notches than in the previous chips, the volume of each notch was lower due to the curved nature of the slope. The sintered and un-sintered chips had an individual notch volume of $0.08mm^3$ while the curved slope chip had 0.078^3. The longer notch with a shallower slope near the edge may have provided less volume for the bubble to form in causing it to rise

further out of the notch than in other configurations. With it further out of the notch it is more likely to merge with a paired bubble and be affected by the flow of incoming fluid.
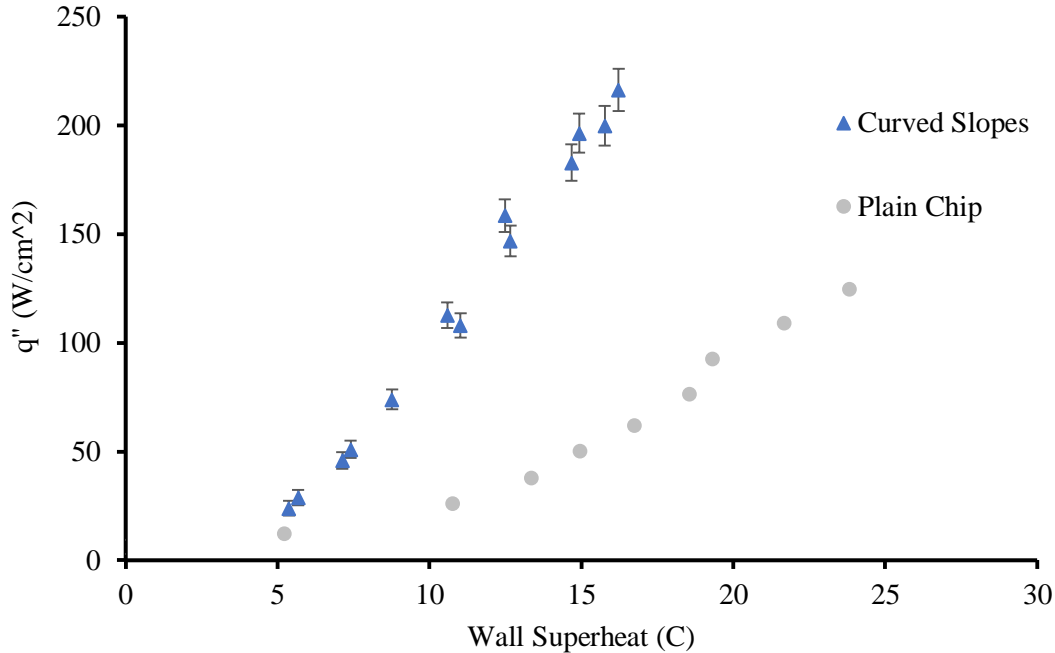
Curved Slopes Notch Chip Boiling Curve

Figure 23 Curved Slopes Notch boiling curve with uncertainty

The final series of chips created included microchannel to greatly increase surface area and fluid flow direction. Three chips where made with different channel and wall widths of 300µm, 400µm, and 500µm. Microchannel chips function well as the channels provide good conditions for vapor nucleation and at high temperatures allow for increased wettability. Each chip was run through the experiment three times in order to obtain reliable data. The 300µm microchannel with notches chip ran into issues with hitting CHF at very low temperatures in comparison to the other chips. As seen in Figure 24 300µm Microchannel with Notches Chip Boiling Curve with Uncertainty Runs 1 and 3 started film boing at lower temperatures while Run 2 was able to achieve much higher temperatures and heat flux. This heat flux is very good in comparison to earlier chip sets but is over taken in efficiency by the 400µm chip which was able to achieve similar heat flux at lower temperatures and did not have issues with reaching CHF early. In all runs of the 400µm chip CHF was not reached and test was not continued to higher temperatures to avoid damaging the equipment. Figure 25 400µm Microchannel with Notches Chip Boiling Curve with Uncertainty shows that the 400µm chip was able to achieve 200 W/cm^2 several degrees below that of the 300µm chip. The 500 µm also performed poorly in comparison to both the 300 µm and 400 µm chips. In all three runs it achieved CHF

at about the same heat flux. Only at lower temperature ranges did it outperform the other two microchannel chips.
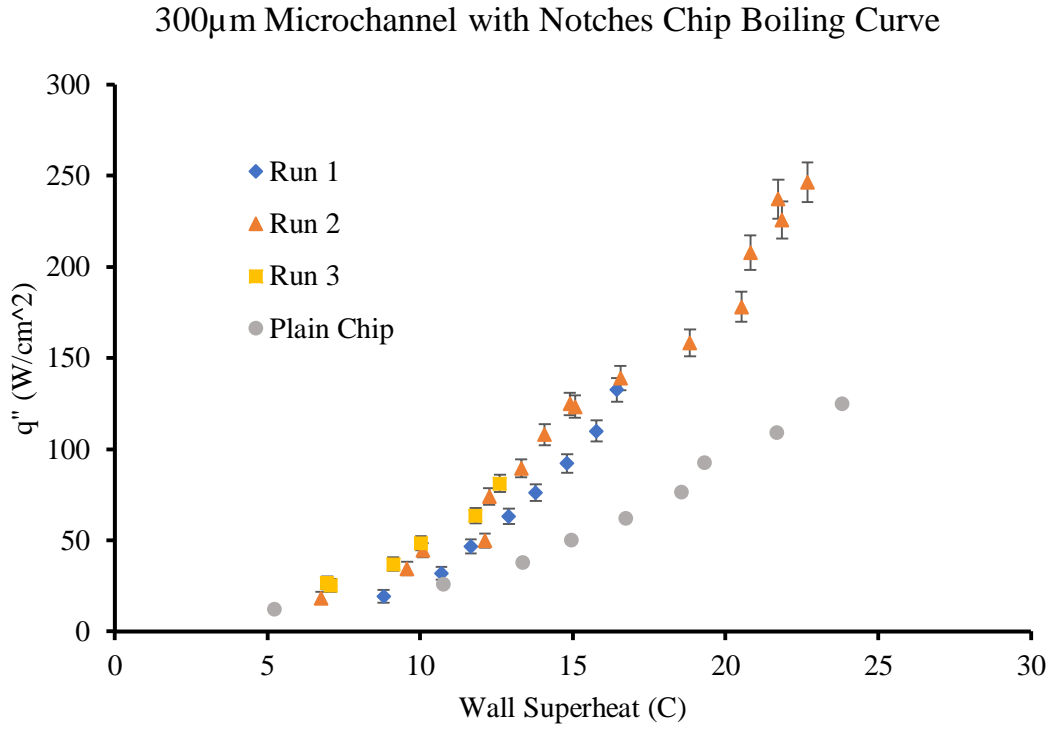

300μm Microchannel with Notches Chip Boiling Curve

Figure 24 300μm Microchannel with Notches Chip Boiling Curve with Uncertainty

400µm Microchannel with Notches Chip Boiling Curve

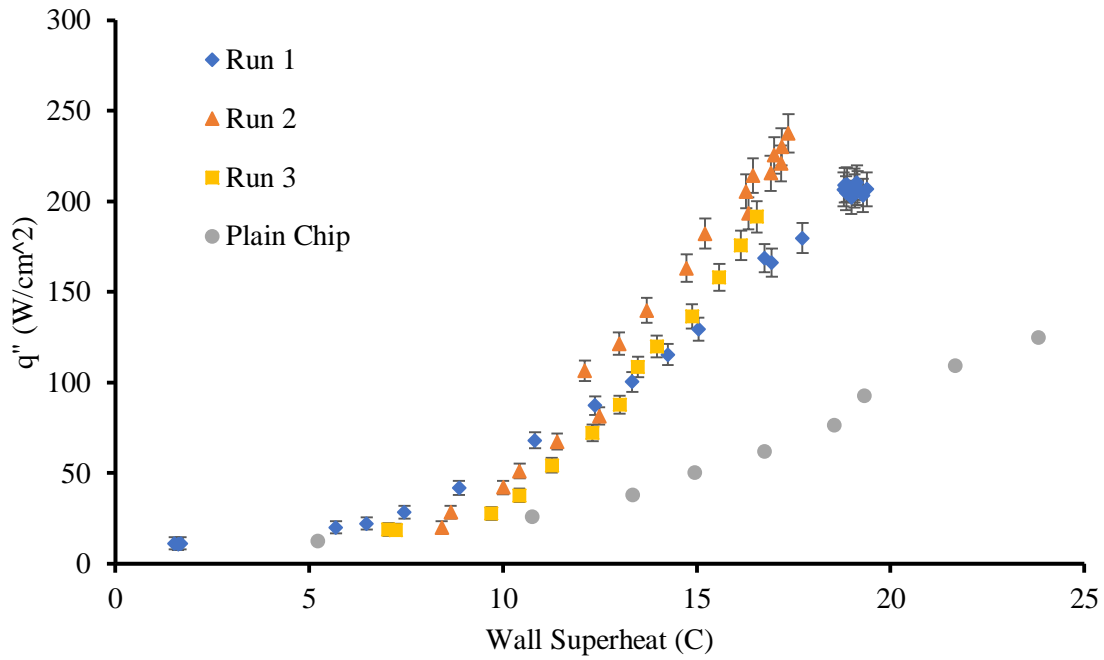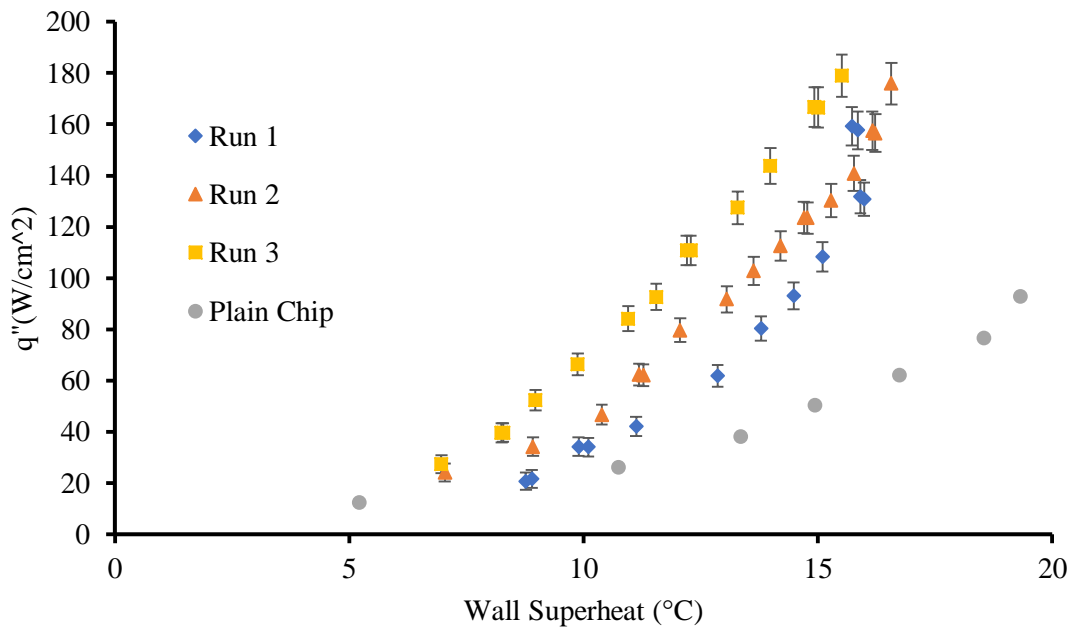*Figure 25 400µm Microchannel with Notches Chip Boiling Curve with Uncertainty*

500µm Microchannel with Notches Chip Boiling Curve

After the completion of the three microchannel chips the integrated heater chip was made using the 400μm chip design. This chips dimensions ended up being much closer to the design specifications than the original 400μm chip seen in the values listed in Table 3 Laser Scanning Microscope Measurments. The tests for this chip followed the same as before except seven runs where performed on this chip. Compared to the other chips this one presented a slowly worsening effectiveness over the first three runs so several more where done to see if this trend continued. After the fourth run the efficiency of the chip stopped going down as can be seen in Figure 27 400μm Microchannel with Notches Integrated Heater Chip Boiling Curve with Uncertainty. The decrease is quite significant and may have been caused by an outside factor. Observing the chip surface with the laser microscope there was an area with a clack raised substance on it. This is believed to be a small amount of melted plastic that had adhered to the surface and burnt onto it during an experimental run. Since this chip was physically attached to the heater block there was no way to remove it after CHF had been achieved. Normally the chip would be raised off the heater block in order to cool it and prevent damage to the plastic gasket on its surface and other parts of the testing apparatus. Since temperatures of the surface achieve 300°C it could have easily melted plastic. A syringe with a rubber tube affixed to it was used to pull out some of the hot water while cooler water was introduced to help keep the system cool. The plastic may have originated from the gasket or the syringe tube and negatively imparted the efficiency as it burnt onto the surface. Both the best and worst run from this chip is displayed on the combined chart in Figure 28 All Chips Boiling Curve Combined. The best efficiency show could be achievable based on trials from previous experiments done with microchannel. Since this chip is more dimensionally accurate to the design, it may have produced better results before becoming contaminated. Also, for consideration of these chips is the aging of the metal due to the elevated temperatures of the metal being cooled by water which can lead to oxidation and alteration of metal properties which can also add to the slowly decreasing efficiency. This chip was still not able to exceed the 250W/cm^2 heat transfer.

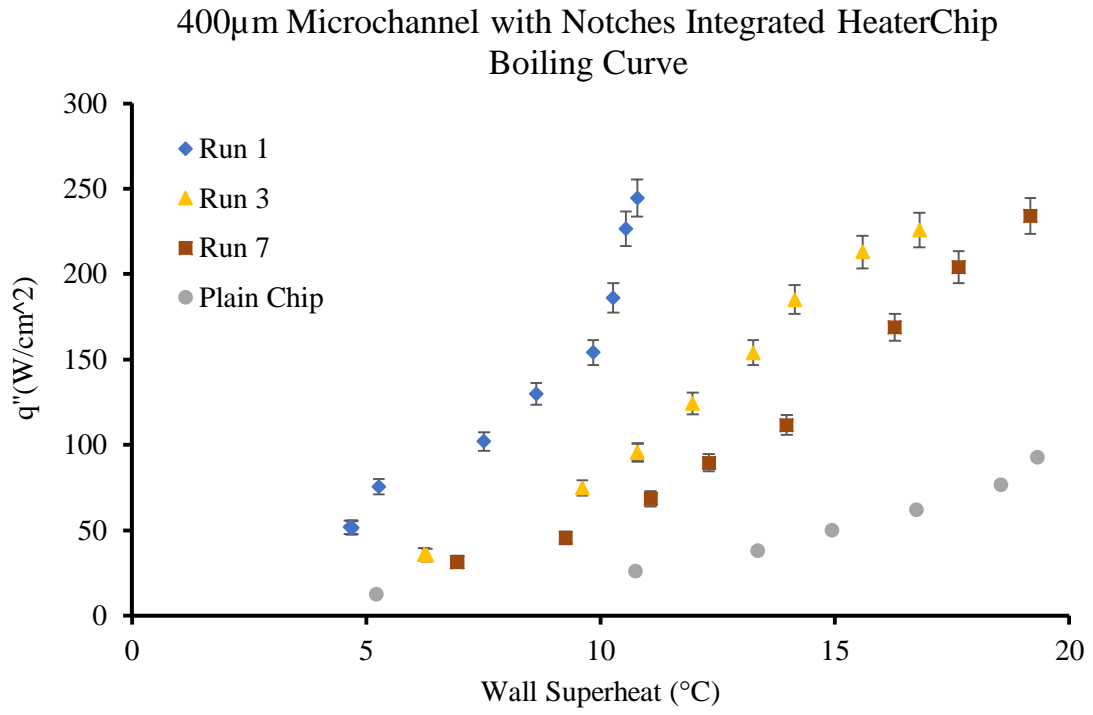*Figure 27 400μm Microchannel with Notches Integrated Heater Chip Boiling Curve with Uncertainty*

All Chips Simplified Boiling Curve

Legend:
- Plain Chip
- 9 Pair
- Staight Slope
- Sintered Staight Slope
- Curved Slopes
- 300μm Microchannel
- 400μm Microchannel
- 500μm Microchannel
- 400μm Integrated Heater
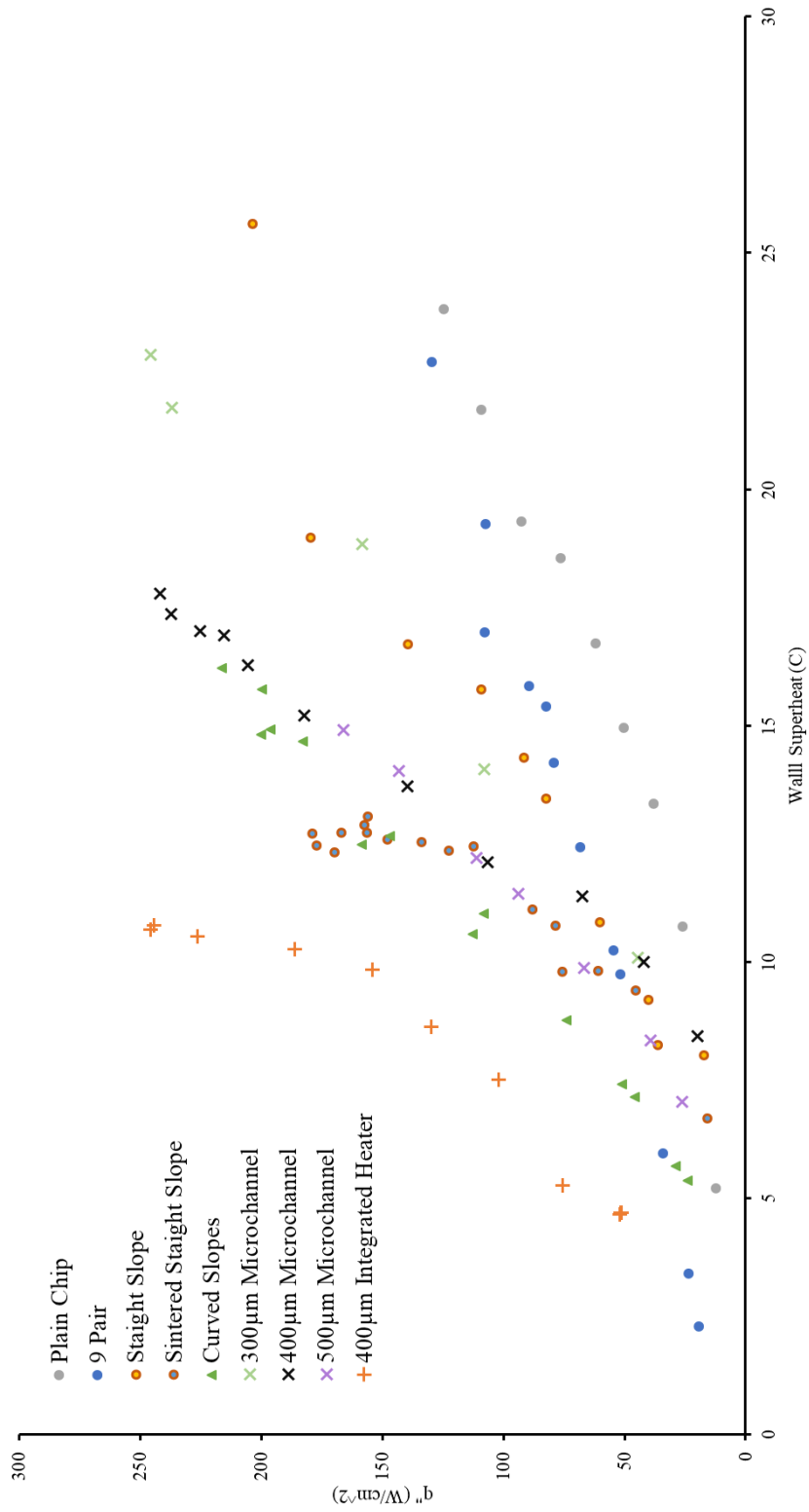
q'' (W/cm^2)

Walll Superheat (C)

Figure 28 All Chips Boiling Curve Combined

36

5.3. High-Speed Video Capture

Figure 29 shows the flow conditions that were theorized to occur from having one flat wall and one angles wall for vapor bubbles to climb up. High-speed footage of the 3 Notch Pair chip showed promising results that mirrored the predicted flow of the individual angled divot nucleating bubbles that can be seen in Figure 31. These bubbles then fused with the other bubble from the pair and soon departed giving evidence to the idea that these nucleation site pairs would promote faster bubble departure while leaving more room for incoming fluid. However, the bubbles seemed to be minimally affected by the slope present and the spacing of the pairs appeared to influence how the bubbles merged instead. The camera also provided good visualization that the bubbles nucleated in their respective pairs uniformly across all chips. Even the microchannel chips showed initial nucleation in the notches inside the microchannels. This showed that the notches had proper dimensions to initiate vapor formation at lower temperatures compared to nucleation that might occur on the surface from the roughness of the chip. It is important that this nucleation start in the desired notch areas so that distinct vapor columns would form leading to the formation of the separate liquid vapor pathways.

High speed of the sintered and un-sintered chips reviled there was some issue with the adjustment made to the spacing between the paired notches. As stated previously the separate pairs of notches were too close to each other while the paired notches were too far. The decision to widen the gap between paired notches was made so applying sinter would be easier. Figure 32 shows the bubbles combining in the liquid pathway. This happened more frequently on the sintered chip.

In all chips at high heat flux, capturing useful images was difficult as the vapor pathways would break down into a single chaotic stream after leaving the surface. At this point the wettability and the chips ability to hold water on the surface became a large factor in increased CHF. This can account for the greater success the 400µm microchannel with notches chip had at elevated temperatures. As previously stated in the initial tests the 400µm microchannel with notches chip never achieved CHF because the pool boiling setup could not increase the heat any further with possible damage to the heaters. While both of the other two microchannel chips hit CHF at relatively low heat fluxes. Due to the 400µm chips success it was the design used to construct a chip with an integrated heater allowing for the experimental setup to increase the temperature further without damaging the electrical set up.

The high-speed photograph also allowed for imaging of bubble departure diameters. Due to the usually non circular shape of the departing bubbles it was assumed that they maintained an ovaloid shape and volume calculations where performed based on this assumption. After the volume was found a radius of a sphere was calculated based on the resulting volume. To find a scale while viewing footage of the bubble development a thin rod was inserted into the plane of focus of the camera and recorded to achieve a known

distance inside the captured footage. The rod measured 0.5mm in diameter and using pixel distances on the images the radii of the vapor bubbles could be found. This was done to achieve a standard departure size for these chips. Each tested footage proved difficult to find uniformly sized vapor bubbles in as they varied greatly on the same chip most likely skewed by the turbulent nature of the boiling. It was found that most vapor bubble during heat fluxes where individual bubbles out be discerned measured between 2.2 and 2.5 mm in diameter and most remained under 3 mm in diameter. This diameter with some additional space added for vapor movement made up the basis for the paired notch spacing from the curved slope chip iteration onward.
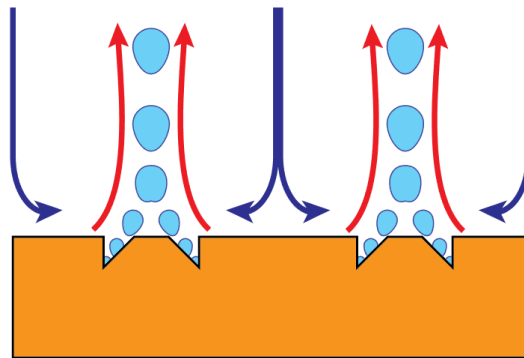
Figure 29 vapor columns forming pathways for cool water
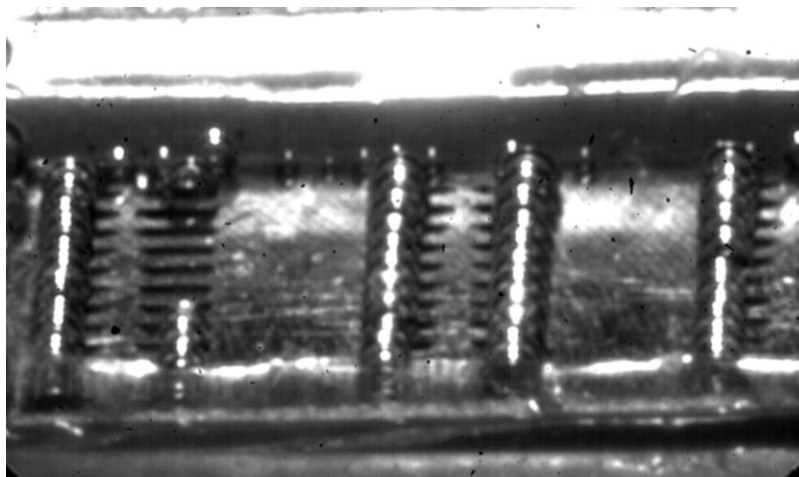
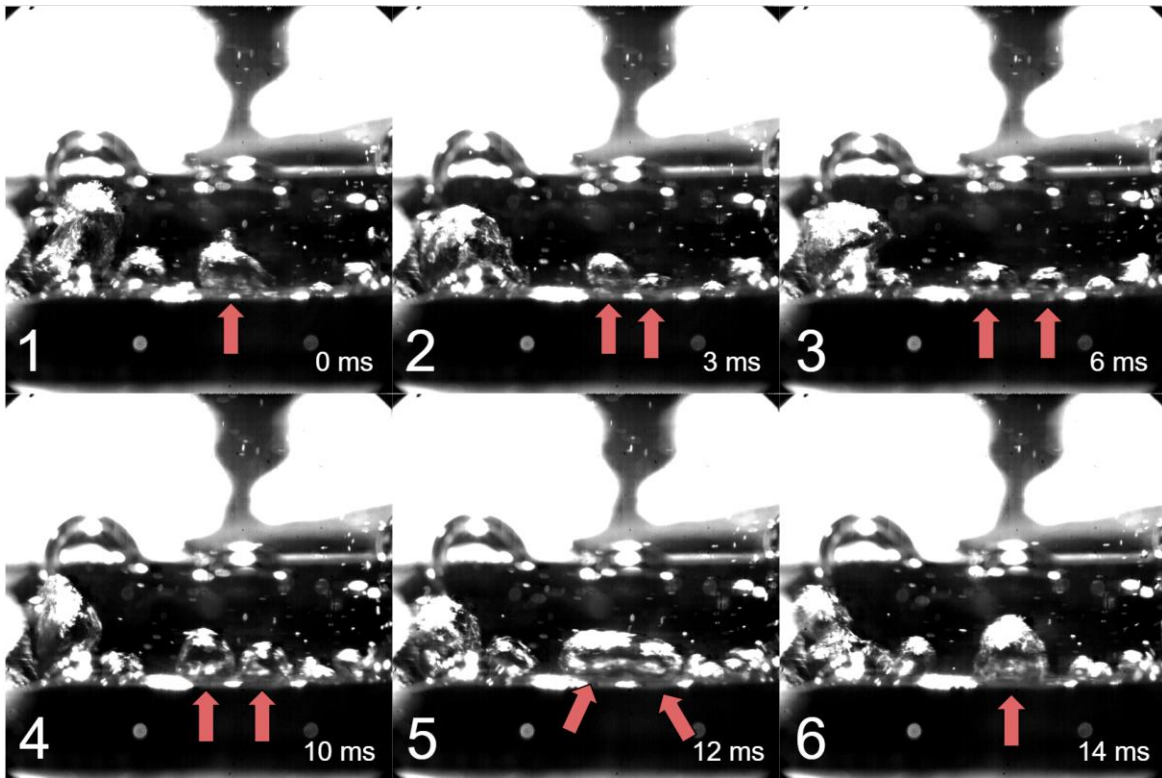*Figure 30 Rows of vapor bubbles sit on curved slopes chip*

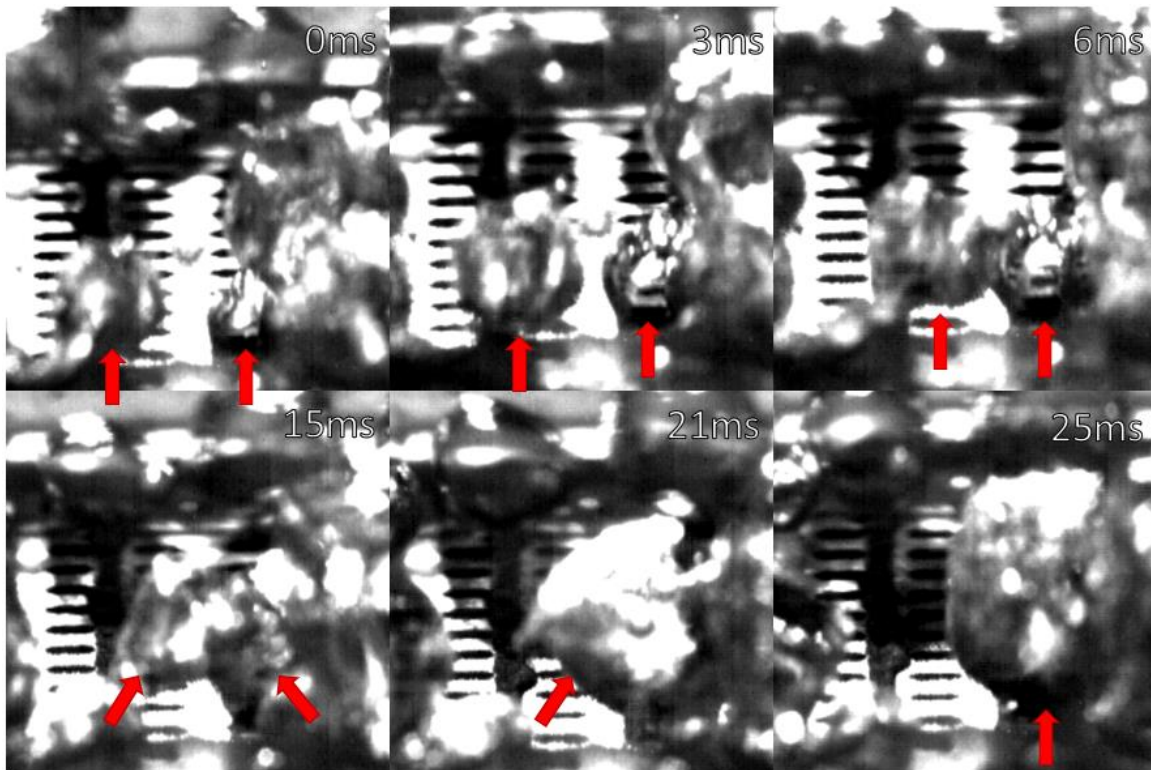*Figure 31 high speed photography of bubbles combining 3 notch pair chip*

Figure 32 High speed photography of bubbles incorrectly combining over liquid pathway on sintered chip

6. Conclusions

The alterations made to the geometry of a heated surface in this study showed heat transfer improvements over plain surfaces in pool boiling. Multiple designs where created based on geometry from previous experimentation with pool boiling and then additional chips where manufactured based on the results from initial designs. High speed imaging confirmed that vapor bubble where nucleating inside individual notches and then condensing into a single lager bubble in the area between the two paired notches. With this information several designs where developed to utilize this phenomenon to promote separate liquid vapor pathways to increase HTC.

First Series of chips, 3 and 9 Notch Pair

1. Angled notches in a surface will promote nucleation and provided they are close enough will allow for vapor bubble merger. This when formed into a pattern can create beneficial separate liquid vapor pathways and can be used to control the movement of the fluid around them.

2. Organized notches that produce vapor jets, even in small number, can increase the effectiveness of nucleate boiling over that of a plain surface or an unorganized roughed up surface as was seen with the 9 notch pair chip. With only 18 small holes added to the results about a 19% increase in HTC.

Second series of chips, Sintered and un-Sintered

1. Sintering provided drastic reduction in temperature needed to produce vapor flow, greatly increasing HTC.

2. Reducing the size of the non-nucleating zone to that of about half the vapor bubble departure diameter negativity impacts the formation of separate liquid vapor pathways. This will lead to chaotic vapor flow at reduced temperatures leading to issues of not being able to reach higher surface temperatures.

Third Chip, Curved Slope Notch

1. Increasing the width of the non-nucleating zone provides better HTC and increases CHF. This and subsequent chips maintained at least a 3mm c.t.c. distance, slightly larger than the size of the departing vapor bubble. Imaging showed this led to better separate liquid vapor pathways.

2. The increased length and decreased volume of the notches may allow for faster removal of newly nucleated bubbles promoting greater heat flux. Since the bubble sit less deeply in the notches, they are influenced more by the fluid motion.

Fourth Series, Microchannels with Notches

1. Microchannel created largely increased surface area and a heat flux. This is due to their ability to allow the surface to be wetted even at higher heat fluxes by giving the fluid a path to travel and store itself out of the way of rising vapor that might prevent its access to the surface.

2. Compared to similar trials that used microchannel of comparable depth that lacked the notches in the base, these ones that included the notch appear to have functioned worse. The microchannels 6 and 8 as seen in Table 1 Dimensions for chips used in and Figure 4 Heat Transfer Coefficient vs Wall Superheat for chips in have dimensions similar to the 300µm and 400µm microchannel with notches chips respectively. They in turn had maximum HTC of 190 and 170 kW/m^2/K while the 300µm and 400µm microchannel with notches chips reached max of 113 and 141 kW/m^2/K as show in Table 5 Summery of all chip's improvement over plain surfaces.

3. If the integrated heater chip functioned reliably and performed like it did in the first run it will have provided an excellent HTC for the dimensions of the chip. Compared to other microchannel tests in Table 1 Dimensions for chips used in and Figure 4 Heat Transfer Coefficient vs Wall Superheat for chips in , it would place higher than a majority of the tested dimensions.

Table 5 Summery of all chip's improvement over plain surfaces sorted by HTC

Chip Name	Critical Heat Flux (W/cm^2)	Percent Improvement	Max HTC (kW/m^2/K)	Percent Improvement
Plain Chip	124.9		52.4	
9 Pair	142.1	13.8	64.1	22.3
Sintered	190.4	52.4	142.9	172.7
500µm Microchannels	191.2	53.1	117.2	123.7
Un-sintered	212.1	69.8	100.6	92.0
Curved Slopes	220.6	76.6	139.6	166.4
400µm Microchannels	242.1	93.8	141.2	169.5
Integrated Heater	245.9	96.9	230.3	339.5
300µm Microchannels	250.4	100.5	112.9	115.5

7. Future Work

The results from this research could help with the usage of minor surface enhancements to increase the efficiency of pool boiling. While there are many other very efficient methods of surface enhancement, they often need high precision manufacturing or coatings that can wear down.

1. Look into the success of the curved slope design and the reason for why this design exceeded microchannels at low temperatures. This design could possibly be reworked to function at even higher surface temperatures. In combination with microchannels, the curved slop could prove very efficient. The integrated heater microchannel design also showed promise in its first run and if the chip could be cleaned or replicated it might perform well compared to other similar designs that have shallow microchannels. The inclusion of these small nucleation zones may boost the efficiency beyond what was seen in the shallow microchannels from [11].

2. Better visualization of the currents in the designs not involving microchannel would be helpful to see how the fluid flow effects the vapor movement and merger if at all. This could be done through the addition of particles to the fluid in order to be able to see the current motion on camera. This may reveal current dead zones that could be better utilized to move fluid more efficiently to the surface and help to detach bubbles at a faster rate.

3. The manufacturing technique used in this study took a significant time to process each chip. Possibly look into faster methods of chip creation either for production or for future research turnaround times. Laser engraving is able to cut fairly intricate designs into copper. Other ablation process exist that may create surfaces with more uniform roughness, which can help eliminate roughness as a factor when studying these types of surface enhancements.

8. References

[1] S. Nukiyama, "The Maximum and Minimum Values of the Heat Q Transmitted from Metal to Boiling Water under Atmospheric Pressure," *International Journal of Heat and Mass Transfer,* vol. 27, no. 7, pp. 959-970, 1984.

[2] E. A. Farber and R. L. Scarab, "Heat Transfer to Water Boiling under," *Transactions of the ASME,* vol. 70, pp. 369-384, 1948.

[3] a. B. J. Mosciki, "Discussion of Heat Transfer From a Platinum Wire Submerged in Water," *Polish Journal of Chemistry (Roczniki Chemii),* vol. 6, p. 321–354, 1926.

[4] J. G. Collier and J. R. Thome, Convective Boiling and Condensation 3rd edition, New York: Oxford University Press, 1994.

[5] R. R. S. Robert C. Hendricks, "Initiation of Cooling due to Bubble Growth on a Heating Surface," National Aeronautics and Space Administration, Washington D.C., 1964.

[6] C.-Y. Han, *THe Mechanism of Heat Transfer in Nucleate Pool Boiling,* Massachusetts : Massachusetts Institute of Technology, 1992.

[7] S. Liter and M. Kaviany, "Pool-boiling CHF enhancement by modulated porous-layer coating: theory and experiment," *International Journal of Heat and Mass Transfer,* vol. 44, no. 22, pp. 4287-4311, 2001.

[8] N. Zuber, *Hydrodynamic Aspec of Heat Transfer,* Los Angeles, California : University of California , 1959.

[9] S. G. Kandlikar and A. Jaikumar, "Pool boiling inversion through bubble induced macroconvection," *Applied Physics Letters,* vol. 110, no. 9, 2017.

[10] S. G. Kandlikar and A. Jaikumar, "Pool boiling enhancement through bubble induced convective liquid flow in feeder microchannels," *Applied Physics Letters,* vol. 108, no. 4, 2016.

[11] D. Cooke and S. Kandlikar, "Effect of open microchannel geometry on pool boiling enhancement," *International Journal of Heat and Mass Transfer,* vol. 55, no. 4, pp. 1004-1013, 2012.

[12] M. Kaviany, Principles of Heat Transfer in Porous Media, New York: Springer, 1999.

[13] A. K. Mostafa Shojaeian, "Pool boiling and flow boiling on micro- and nanostructured surfaces," *Experimental Thermal and Fluid Science,* vol. 63, pp. 45-73, 2015.

[14] S. J. Penley and R. A. Wirtz, "Correlation of Subatmospheric Pressure, Saturated, Pool Boiling of Water on a Structured-Porous Surface," *Journal of Heat Transfer,* vol. 133, no. 4, p. 11, 2011.

[15] T. Chen, "An experimental investigation of nucleate boiling heat transfer froman enhanced cylindrical surfac," *Applied Thermal Engineering,* vol. 59, pp. 355-361, 2013.

[16] X. Wang, Z. Wang and Q. Chen, "Research on manufacturing technology and heat transfer characteristics of sintered porous surface tubes," *Advanced Materials Research,* Vols. 97-101, pp. 1161-1165, 2010.

[17] C. M. Patil and S. G. Kandlikar, "Pool boiling enhancement through microporous coatings selectively electrodeposited on fin tops of open microchannels," *International Journal of Heat and Mass Transfer,* vol. 79, pp. 816-828, 2014.

[18] S. G. Kandlikar, "A Theoretical Model to Predict Pool Boiling CHF Incorporating Effects of Contact Angle and Orientation," *J. Heat Transfer,* vol. 123, no. 6, pp. 1071-1079, 2001.

[19] S. G. Kandlikar, "Controlling bubble motion over heated surface through evaporation momentum force to enhance pool boiling heat transfer," *Applied Physics Letter,* vol. 102, 3013.

[20] A. Hayes, "Additive Manufactured Microstructures and Designs for High Heat Flux Dissipation During Pool Boiling," Rochester Institute of Technology, Rochester, 2018.

[21] A. R. Betz, J. Xu, H. Qiu and D. Attinger, "Do surfaces with mixed hydrophilic and hydrophobic areas enhance pool boiling?," *Applied Physics Letters,* vol. 97, no. 14, 2010.

[22] P. A. R. a. S. G. Kandlikar, "Pool boiling enhancement through contact line augmentation," *Applied Physics Letter,* vol. 110, no. 20, 2017.

[23] S. G. Kandlikar, M. E. Steinke and P. Balasubramanian, "Single-Phase Flow Characteristics and Effect of Dissolved Gases on Heat Transfer Near Saturation Conditions in Microchannels," in *ASME 2002 International Mechanical Engineering Congress and Exposition*, New Orleans, Louisiana, 2002.

[24] A. Walunj and A. Sathyabhama, "Influence of surface roughness on pool boiling heat transfer," in *IOP Conference Series: Materials Science and Engineering 402*, 2018.

[25] B. J. Jones, J. P. McHale and S. V. Garimella, "The Influence of Surface Roughness on Nucleate Pool Boiling Heat Transfer," *Journal of Heat Transfer,* vol. 131, no. 12, p. 14, 2009.

[26] V. Mejia, "Pool Boiling Heat Transfer Surface Enhancement using Electrodeposition with Non-Electrolyte Bath," Rochester Institute of Technology, Rocester, 2015.